Computers and Structures 260 (2022) 106704

Contents lists available at ScienceDirect

Computers and Structures

journal homepage: www.elsevier.com/locate/compstruc

An enhancement of overlapping finite elements

Sungkwon Lee, Klaus-Jürgen Bathe *

Department of Mechanical Engineering, Massachusetts Institute of Technology, Cambridge, MA 02139, USA

ARTICLE INFO

Article history:
Received 11 September 2021
Accepted 23 October 2021

Keywords:
Finite elements
Overlapping elements
Distortion-insensitivity
Conditioning of equations
Stability and accuracy
AMORE

ABSTRACT

We present a novel further development of overlapping finite elements. The formulation of the enhanced elements is based on the earlier published elements but has an important new ingredient which renders the enhanced formulation more effective with respect to the evaluation of the element matrices and the solution of the governing finite element equations. The novel ingredient is that the elements are no longer based on a function used in meshless solution schemes; hence the elements provide more generality and ease of use. We first give the formulation which is applicable to two- and three-dimensional analyses of solids, give new insights, and then present an evaluation considering the required numerical integration, geometric distortion-insensitivity and the conditioning of the resulting finite element equations. In the study of the element characteristics, we also give some illustrative example solutions that show the performance of the elements in linear static analyses of two- and three-dimensional solids.

1. Introduction

Finite element analysis is now widely used in engineering practice. However, the potential of finite element analysis has not been fully exploited yet, frequently due to difficulties in meshing of the analysis domain due to its geometric complexity [1]. To circumvent the effort of meshing, various meshless methods have been proposed [2,3]. Meshless methods provide much flexibility in discretization, but the use of such techniques, those not involving numerical factors for stability, in practice is often restricted by the prohibitively expensive numerical integrations [1,4–6].

In our earlier papers [7–11], we proposed the use of overlapping finite elements (OFE) and the AMORE scheme for "automatic meshing with overlapping and regular elements". The development of the overlapping finite elements was inspired by the formulation of the method of finite spheres in which the Shepard function is used with a radius for each sphere [2,4,7]. However, quite different from the use of spheres, the overlapping elements we proposed use no rational functions, or their derivatives, in the element matrices [10,11], which renders the numerical integration much more tractable. An overlapping element has also the same element connectivity as the traditional element. Hence the element can be embedded into a mesh of traditional elements and can directly be used in the same way as a traditional finite element. Another important point is that the overlapping elements maintain polynomial completeness when distorted, and hence are quite distortion-insensitive [1,11].

Based on these element behaviors, the AMORE scheme fills the analysis domain mostly with traditional geometrically-undistorted elements – which are effective because they are not distorted [12] – and uses the overlapping finite elements only to discretize regions where distorted elements need be used. The AMORE scheme therefore spans an effective mesh quite efficiently over the complete geometric domain to be analyzed.

However, the earlier proposed overlapping element formulations contain some ingredients that might be improved. Firstly, the construction of the displacement interpolation is not as effective as we desire. Secondly, the use of a radius pertaining to each node would ideally not be necessary, and thirdly the condition number of the resulting stiffness matrix can become large, in particular when a large radius for the nodes is used.

Our improvements in the formulation of the overlapping finite elements presented in this paper address these three points. A Shepard function is no longer used to construct the displacement interpolations which renders the formulation more efficient, and a radius for each node is no longer used which also has a beneficial effect on the conditioning of the equations. Furthermore, the same element formulation is used for any of the basic low-order elements we consider in this paper for two- and three-dimensional analyses.

A major issue in generalizing or enriching finite element discretizations is that the resulting equations may be linearly dependent. For example, the generalized finite element method with polynomial enrichments could suffer from the problem of linear

* Corresponding author.
E-mail address: kjb@mit.edu (K.J. Bathe).

https://doi.org/10.1016/j.compstruc.2021.106704
0045-7949/

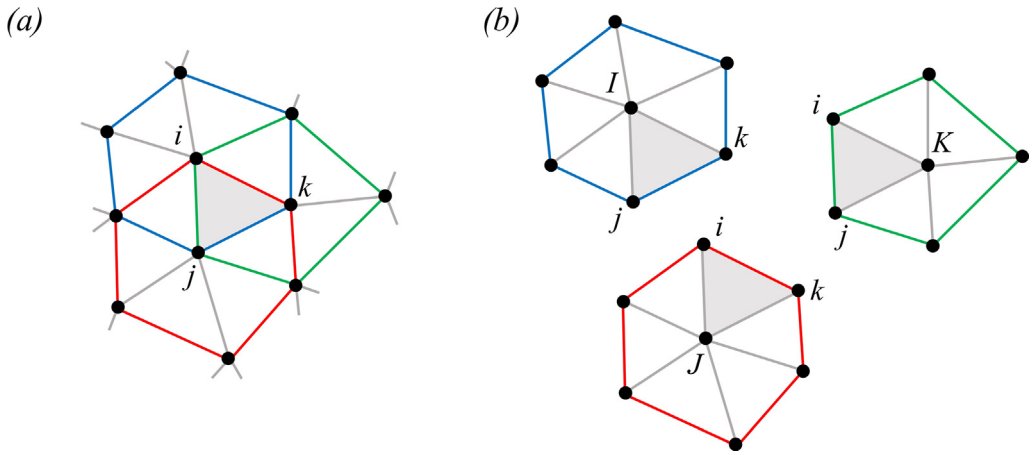

Fig. 1. Triangularization and overlapping elements; (a) The triangular element of three nodes *i, j, k* is part of three overlapping polygonal elements; (b) The three polygonal elements are denoted by the capital letters *I, J, K*.

dependency [13–16]. Various approaches have been proposed to address this issue. In an early approach, special solvers were used to solve the linearly dependent equations [13]. More recently, special element interpolation functions have been used with discontinuities in derivatives resulting in strain jumps within the elements [15–18]. These strain discontinuities within the elements are, however, not desirable and do not lead to optimal solutions of physical problems with smooth strain variations, and we consider in this paper only the analyses of such physical problems.

In the method of finite elements with interpolation covers [19–21], the linear dependency is removed by suppressing all cover degrees of freedom on the boundaries with prescribed displacements. There is a loss of solution accuracy near such boundaries, which however with a fine enough mesh is acceptable. The technique is simple but only applicable when the 3-node triangular or 4-node tetrahedral elements are used for two- and three-dimensional analyses, respectively.

The governing equations of the overlapping finite elements that we introduce in this paper exhibit no linear dependency, and the conditioning of the equations is reasonable. The element displacement interpolation functions are also smooth within an element and result into good solution accuracy. Further, we need not remove all degrees of freedom at the boundaries with prescribed displacements to reach a reasonable conditioning of the stiffness matrix.

In the following, we first introduce the new formulation in Section 2 and present numerical aspects in Section 3. Then in Sections 4 and 5, using the new formulation and the AMORE scheme, we solve various linear static problems and show the effectiveness of the new elements in, both, the accuracy of solutions and the conditioning of the governing equations. Our concluding remarks are given in Section 6.

2. Formulation of the enhanced overlapping finite elements

We give in this section the basic equations of the formulation focusing on the interpolations used and also discuss the imposition of the displacement boundary conditions and the use of the elements in the AMORE scheme.

2.1. Interpolations used

Given a linear elasticity problem, we discretize in the overlapping finite element method a displacement component u (e.g., x-direction displacement) as follows.

$$u(\boldsymbol{x}) = \sum_{I=1}^{N} h_I \psi_I \tag{1}$$

Table 1
Numerical integration schemes used for the new overlapping finite elements; GQ denotes the Gauss quadrature; the numbers in brackets give the refs.

Element	Linear basis	Bilinear basis	Quadratic basis
3-Node triangular	6 [22]	9 [22]	12 [22]
4-Node quadrilateral	3 × 3 GQ	4 × 4 GQ	5 × 5 GQ
4-Node tetrahedral	11 [23]	17 [24]	29 [24]
8-Node brick	3 × 3 × 3 GQ	4 × 4 × 4 GQ	5 × 5 × 5 GQ

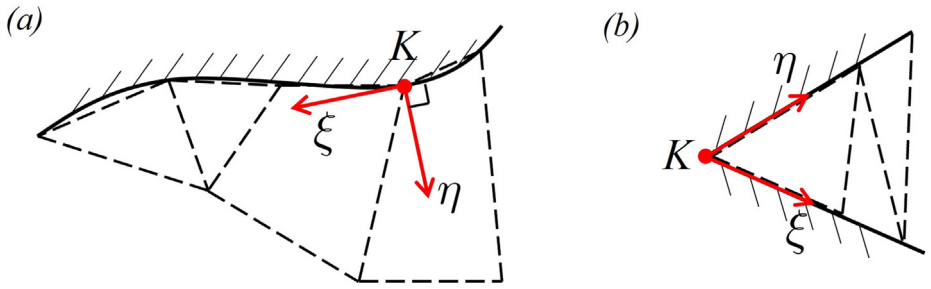

Fig. 2. Local coordinates used for a node at a Dirichlet boundary; (a) Node *K* located at a point of a smooth boundary; (b) Node *K* located at a point of a non-smooth boundary; dotted lines represent element edges.

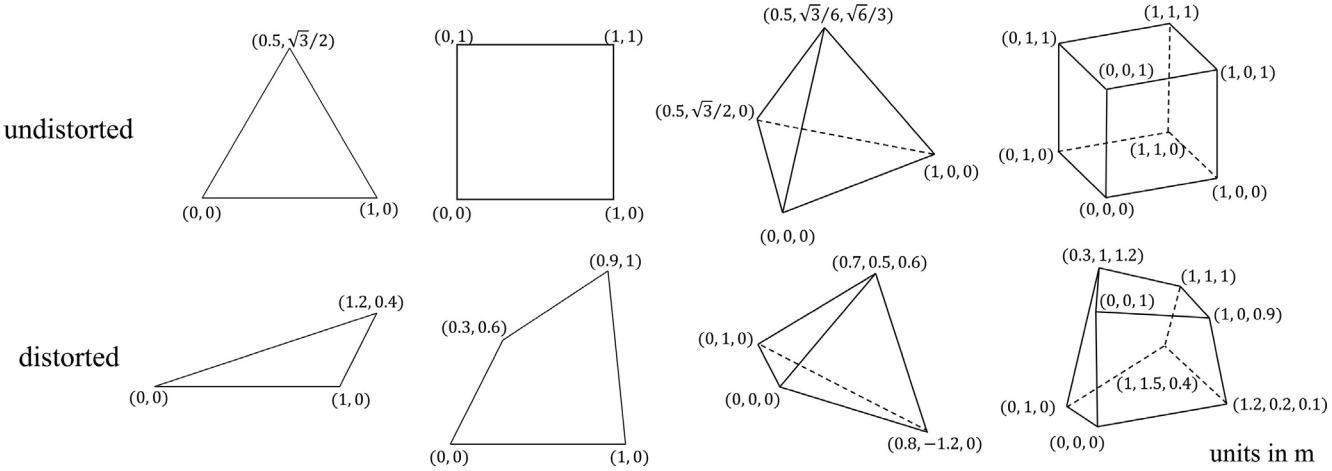

Fig. 3. Undistorted and distorted elements used in the zero energy mode test; the Cartesian coordinates of nodes are given.

Table 2
Zero energy mode test on undistorted elements including the eigenvalues which we consider to be zero (the very small numbers being due to round-off in the numerical solutions); the first, second, and third rows are for the linear, bilinear, and quadratic bases.

Element	$\lambda_{1,\ \text{smallest}}$	λ_2	λ_3	λ_4	λ_5	λ_6	λ_7	λ_8
3-Node triangular	-7.12×10^{-8}	8.66×10^{-9}	1.84×10^{-7}	5.47×10^{5}	5.47×10^{5}	8.38×10^{5}	1.35×10^{6}	1.35×10^{6}
	-3.39×10^{-7}	1.08×10^{-7}	3.64×10^{-7}	2.21×10^{2}	5.20×10^{2}	4.32×10^{4}	4.85×10^{4}	4.34×10^{5}
	-4.88×10^{-8}	1.04×10^{-8}	1.66×10^{-7}	1.28×10^{1}	1.28×10^{1}	2.90×10^{1}	5.08×10^{1}	6.17×10^{1}
4-Node quadrilateral	-3.23×10^{-7}	7.77×10^{-8}	2.21×10^{-7}	4.73×10^{5}	4.73×10^{5}	6.15×10^{5}	1.07×10^{6}	1.35×10^{6}
	-1.97×10^{-7}	-1.06×10^{-8}	1.03×10^{-7}	2.75×10^{4}	2.75×10^{4}	2.87×10^{4}	5.36×10^{4}	8.47×10^{4}
	-4.29×10^{-7}	-5.68×10^{-8}	-1.97×10^{-8}	1.41×10^{2}	1.41×10^{2}	4.66×10^{2}	4.66×10^{2}	1.61×10^{3}
4-Node tetrahedral	-6.32×10^{-7}	-3.28×10^{-7}	-3.08×10^{-7}	-3.35×10^{-8}	1.61×10^{-7}	5.33×10^{-7}	8.35×10^{4}	8.35×10^{4}
	-4.68×10^{-7}	-2.60×10^{-7}	-1.17×10^{-7}	9.38×10^{-8}	1.82×10^{-7}	4.08×10^{-7}	1.66×10^{1}	2.37×10^{1}
	-1.16×10^{-9}	1.30×10^{-9}	9.43×10^{-9}	4.09×10^{-8}	4.22×10^{-8}	6.92×10^{-8}	6.51×10^{-1}	2.57×10^{0}
8-Node brick	-6.64×10^{-8}	-5.16×10^{-8}	-1.76×10^{-8}	1.24×10^{-8}	6.48×10^{-8}	7.21×10^{-8}	4.43×10^{4}	5.01×10^{4}
	-5.64×10^{-8}	-3.38×10^{-8}	-2.87×10^{-8}	2.09×10^{-8}	2.70×10^{-8}	7.13×10^{-8}	1.25×10^{3}	1.25×10^{3}
	-7.43×10^{-8}	-1.52×10^{-8}	-7.82×10^{-9}	1.66×10^{-8}	9.06×10^{-8}	1.08×10^{-7}	1.45×10^{1}	1.45×10^{1}

Table 3
Zero energy mode test on distorted elements including the eigenvalues which we consider to be zero (the very small numbers being due to round-off in the numerical solutions); the first, second, and third rows are for the linear, bilinear, and quadratic bases.

Element	$\lambda_{1,\ \text{smallest}}$	λ_2	λ_3	λ_4	λ_5	λ_6	λ_7	λ_8
3-Node triangular	-2.54×10^{-7}	3.11×10^{-8}	4.02×10^{-7}	7.58×10^{4}	1.43×10^{5}	2.90×10^{5}	5.24×10^{5}	9.76×10^{5}
	-2.09×10^{-7}	-4.66×10^{-8}	1.94×10^{-7}	5.49×10^{1}	8.55×10^{1}	4.86×10^{3}	1.33×10^{4}	1.19×10^{5}
	-3.09×10^{-7}	4.23×10^{-9}	1.49×10^{-7}	6.21×10^{-1}	2.61×10^{0}	5.00×10^{0}	5.61×10^{0}	3.94×10^{1}
4-Node quadrilateral	-4.33×10^{-7}	2.01×10^{-8}	1.20×10^{-7}	4.28×10^{5}	4.46×10^{5}	5.69×10^{5}	8.14×10^{5}	1.50×10^{6}
	-2.56×10^{-7}	2.40×10^{-8}	2.57×10^{-7}	1.76×10^{4}	1.98×10^{4}	2.98×10^{4}	3.50×10^{4}	1.60×10^{5}
	-1.31×10^{-7}	8.02×10^{-8}	3.11×10^{-7}	1.77×10^{2}	1.93×10^{2}	2.83×10^{2}	3.83×10^{2}	1.90×10^{3}
4-Node tetrahedral	-2.81×10^{-6}	-9.16×10^{-7}	-5.99×10^{-7}	2.25×10^{-7}	4.58×10^{-7}	6.41×10^{-7}	2.76×10^{3}	3.11×10^{3}
	-1.64×10^{-6}	-2.91×10^{-7}	-6.76×10^{-8}	1.76×10^{-7}	5.40×10^{-7}	1.68×10^{-6}	1.18×10^{0}	1.48×10^{0}
	-1.94×10^{-7}	-5.27×10^{-8}	-3.77×10^{-8}	4.90×10^{-8}	1.53×10^{-7}	1.96×10^{-7}	4.37×10^{-2}	6.33×10^{-2}
8-Node brick	-9.71×10^{-8}	-8.22×10^{-9}	-8.06×10^{-9}	1.40×10^{-8}	7.15×10^{-8}	1.57×10^{-7}	4.00×10^{4}	4.54×10^{4}
	-4.64×10^{-8}	-1.71×10^{-8}	2.87×10^{-8}	5.60×10^{-8}	7.31×10^{-8}	1.19×10^{-7}	3.44×10^{2}	4.00×10^{2}
	-1.02×10^{-7}	-9.21×10^{-8}	-3.44×10^{-9}	9.21×10^{-9}	1.53×10^{-8}	1.62×10^{-7}	4.43×10^{1}	4.83×10^{1}

where h_I is the traditional low-order finite element shape function, N is the number of nodes of an element, and ψ_I is the field "corresponding to the polygonal element I associated with node I", see Fig. 1. For ψ_I, we use

$$\psi_I = \sum_{K=1}^{m} \phi_K^I \, u_K \tag{2}$$

where m is the number of nodes of the polygonal element, we need to construct ϕ_K^I, and u_K is the unknown nodal basis function for node K. We consider in this paper u_K to be a polynomial, but other suitable functions can also be used.

The approach in this interpolation corresponds to an "element-overlapping" which we can interpret physically. Let us consider a triangular element with three nodes i, j, k, hence $N = 3$, see Fig. 1.

The element is part of polygonal elements consisting of triangular elements. We label the polygonal element with center node *I*, which is physically at the same location as node *i*, to be the polygonal element *I*. Similarly, we label the polygonal elements with center nodes *J* and *K* as the polygonal elements *J* and *K*, respectively.

Assume that ψ is the displacement component considered here and that using Eq. (2) we interpolate ψ over each polygonal element *I*, *J*, *K*. Then for the polygonal element *I* we use $m = 7$ in Eq. (2) since it has seven nodes, and similarly for the interpolations for the polygonal elements *J* and *K*. In Eq. (1) we superpose these three interpolations of the three polygonal elements; hence the interpolation for the triangular element with nodes *i, j, k* corresponds to the overlapping of three polygonal elements. We call this triangular element an *overlapping finite element*. Since we use in Eq. (1) the interpolation functions h_I, we achieve that the displacement assumption is localized to the triangular element with nodes *i, j, k* and the displacements along the edges of the triangular element are continuous over a patch of such triangular elements.

Hence Eq. (2) reduces to

$$\psi_I = \sum_{K=1}^{N} \phi_K^I \, u_K \tag{3}$$

where *N* is the number of nodes of the overlapping finite element, here $N = 3$. The same procedure is used to construct other overlapping finite elements. The use of Eq. (3) was introduced in Ref. [10].

The key in this interpretation is to think of I in Eq. (1) as "varying over the three element nodes of the 3-node triangular element with each node representing a polygonal element".

An important step in the formulation is to choose effective interpolation functions ϕ_K^I. In earlier developments, see Refs. [10,11], we used

$$\phi_K^I = \sum_{i=1}^{M} \hat{h}_i \, \hat{\phi}_{Ki}^I \tag{4}$$

where the $\hat{h}_i$ is the shape function of a traditional element of the same geometry as the element formulated to allow a higher-order variation for ϕ_K^I, and $\hat{\phi}_{Ki}^I$ is the nodal value for the function (note that in this equation *i* is simply a dummy variable). For example, for the formulation of the 3-node overlapping element we used the traditional interpolation functions of the 6-node triangle, hence $M = 6$ in Eq. (4), and used the Shepard function for the values of $\hat{\phi}_{Ki}^I$ [10]. However, any suitable function can be interpolated, and we use in our current work a function defined by the value of β as given in Appendix A, which is computationally more effective.

Our overlapping finite element formulation of course satisfies – as does the traditional finite element formulation – the partition of unity,

$$u(\boldsymbol{x}) = \sum_{I=1}^{N} h_I \psi_I = \sum_{I=1}^{N} h_I \left(\sum_{K=1}^{N} \phi_K^I \, u_K \right) = \sum_{K=1}^{N} \left(\sum_{I=1}^{N} h_I \, \phi_K^I \right) u_K$$
$$= \sum_{K=1}^{N} \rho_K \, u_K \tag{5}$$

where ρ_K satisfies $\sum_{K=1}^{N} \rho_K = 1$. By virtue of the mathematical relation between the low-order and corresponding higher-order elements [12], we can obtain the following relation from Eqs. (4) and (5) for the improved elements (see Appendix B)

$$\rho_K = h_K + \beta \sum_J (h_J - h_K) \hat{h}_{JK} \tag{6}$$

where *J* is an element node of the overlapping element directly connected to node *K* and $\hat{h}_{JK}$ represents the element function of the

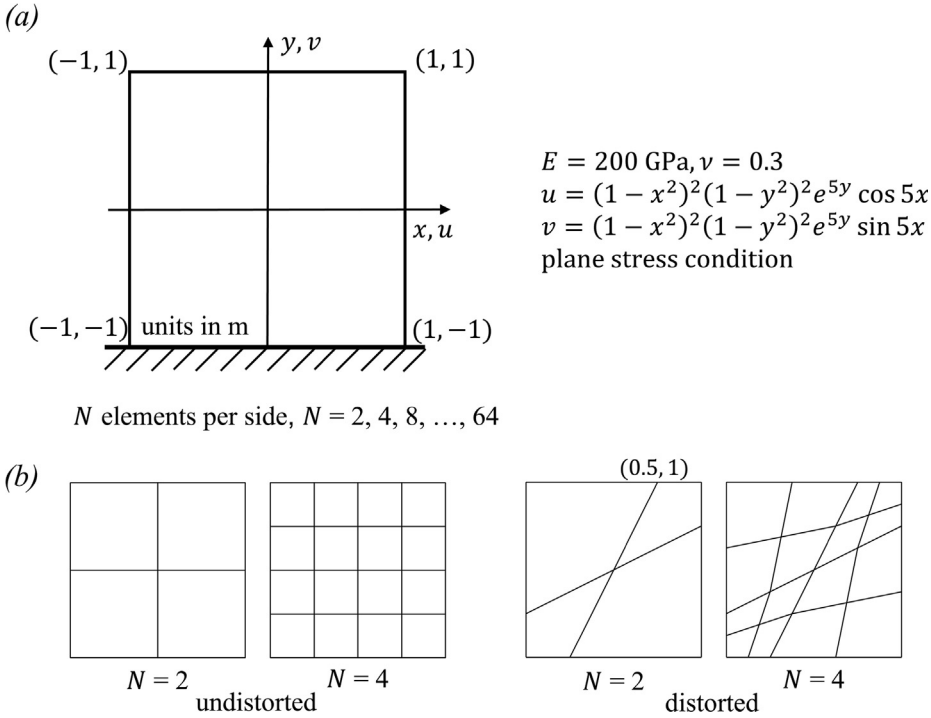

Fig. 4. Two-dimensional adhoc problem; (a) Description of the adhoc problem; (b) Meshes used; the mesh refinement is performed by splitting the edges of an element in half and generating four elements from the element.

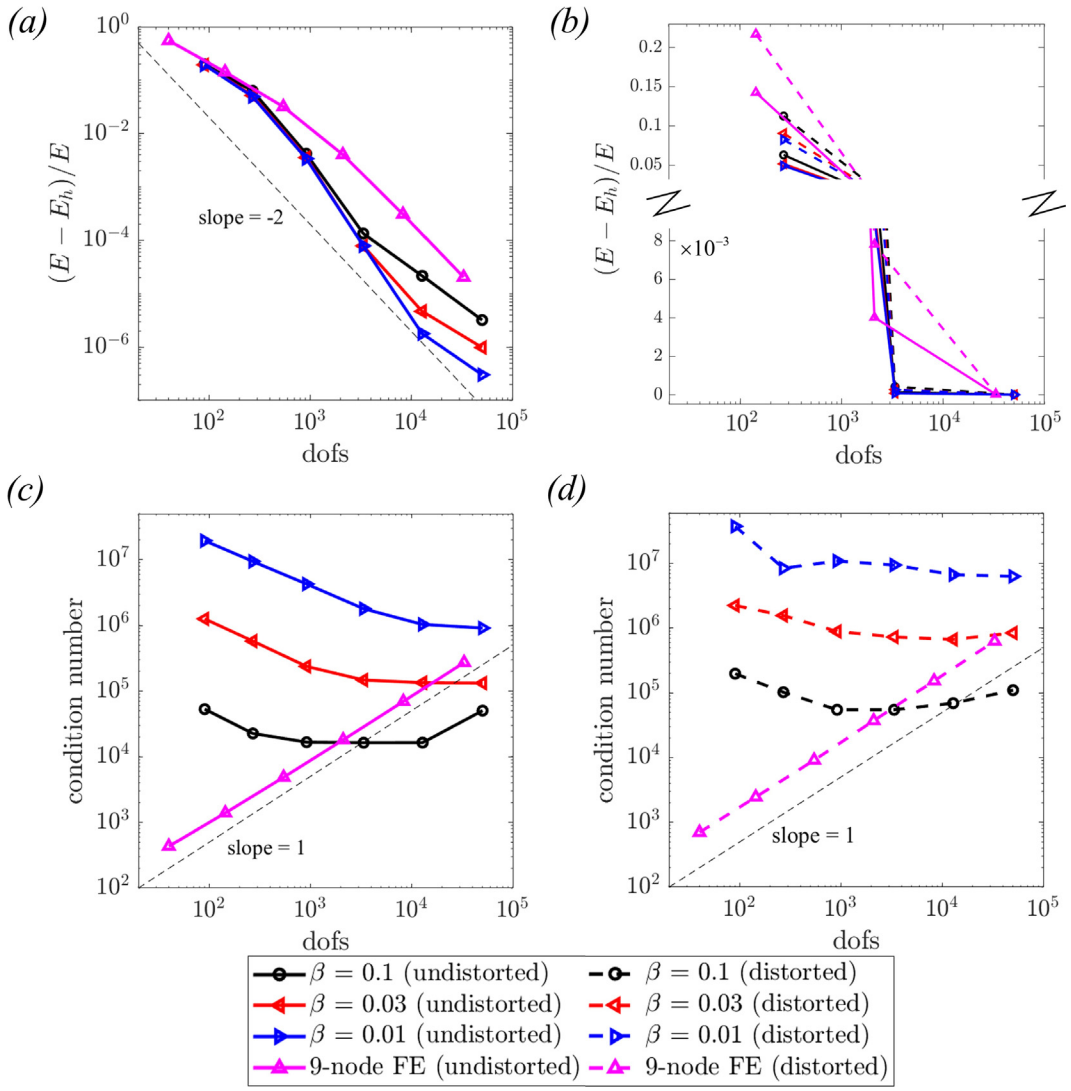

Fig. 5. Adhoc problem solved using the new 4-node quadrilateral overlapping element with the quadratic basis and the traditional 9-node finite element; (a) Convergence of strain energy using undistorted meshes ($N = 2, 4, 8, \ldots, 64$); (b) Comparison between the errors obtained using the undistorted and distorted meshes ($N = 4$, 16, and 64); note that the y-axis uses the linear scale; (c) Change of condition number with refinement of the undistorted mesh; (d) Change of condition number with refinement of the distorted mesh.

mid-side node located between nodes J and K. The function ρ_K is hence cubic along the element edges, and β determines the magnitude of the cubic terms. Note that $\beta = 0$ results in the finite element method with interpolation covers [19–21].

Considering the nodal polynomial u_K in a three-dimensional analysis, for a Cartesian coordinate system $\boldsymbol{x} = (x, y, z)$, we have

$$u_K = a_{K1} + a_{K2}\frac{(x-x_K)}{h} + a_{K3}\frac{(y-y_K)}{h} + a_{K4}\frac{(z-z_K)}{h} + \cdots \tag{7}$$

where a_{Ki} is the unknown variable, $\boldsymbol{x}_K = (x_K, y_K, z_K)$ of node K, and h is equal to $\max_{J \in \mathscr{M}} ||\boldsymbol{x}_J - \boldsymbol{x}_K||/2$ where $\mathscr{M}$ is the set of nodes that are contained in the overlapping polygonal element of node K. For example, when the bilinear polynomial basis is employed we use

$$\begin{aligned} u_K = {} & a_{K1} + a_{K2}\tfrac{(x-x_K)}{h} + a_{K3}\tfrac{(y-y_K)}{h} + a_{K4}\tfrac{(z-z_K)}{h} \\ & + a_{K5}\tfrac{(x-x_K)(y-y_K)}{h^2} + a_{K6}\tfrac{(y-y_K)(z-z_K)}{h^2} + a_{K7}\tfrac{(z-z_K)(x-x_K)}{h^2} \end{aligned} \tag{8}$$

Of course, when considering an analysis in two dimensions, we simply ignore all terms involving the third direction. The physical coordinates x, y, z are interpolated using the natural coordinates as when using the low-order finite element.

Our new overlapping finite element has the following properties.

- The element is isotropic.
- The element is compatible with adjacent elements and provides an element-internal continuous strain field.
- The element passes the patch test provided the nodal basis function includes the linear polynomials.
- Different overlapping elements in a patch (e.g., 3-node and 4-node elements) are compatible if we use the same value of β for each element.
- When the p-th order polynomial basis is used, the element can exactly reproduce any p-th order polynomial.

We discuss below (see Section 3) also the stability of the element, that is, in discretizations using the element we must not have a linear dependency of the governing equations.

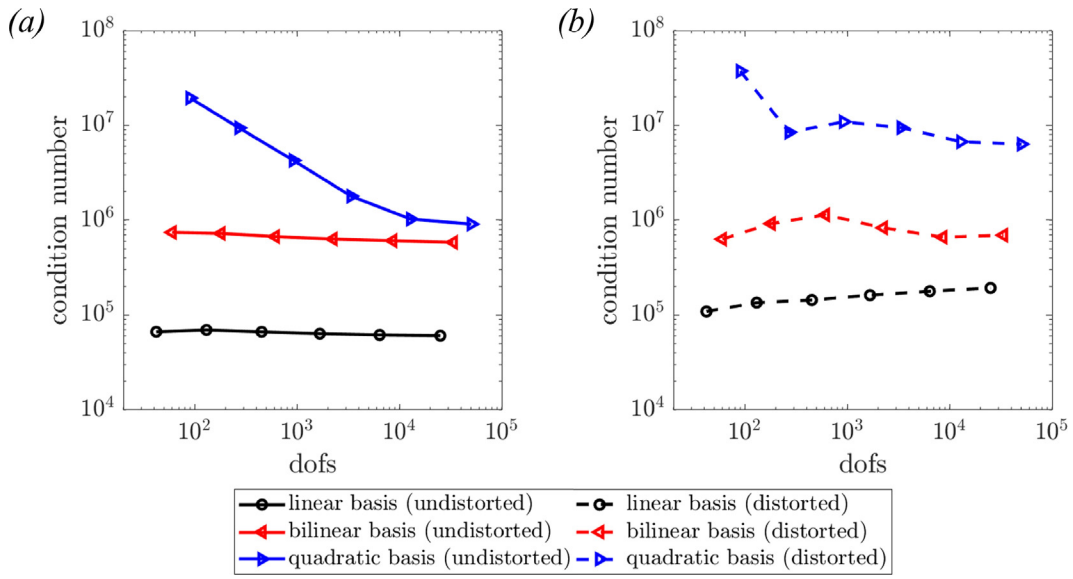

Fig. 6. Effect of the order of polynomial basis on the condition number; the new 4-node quadrilateral overlapping element with $\beta = 0.01$ is used in the undistorted and distorted meshes; (a) Change of condition number with refinement of the undistorted mesh; (b) Change of condition number with refinement of the distorted mesh.

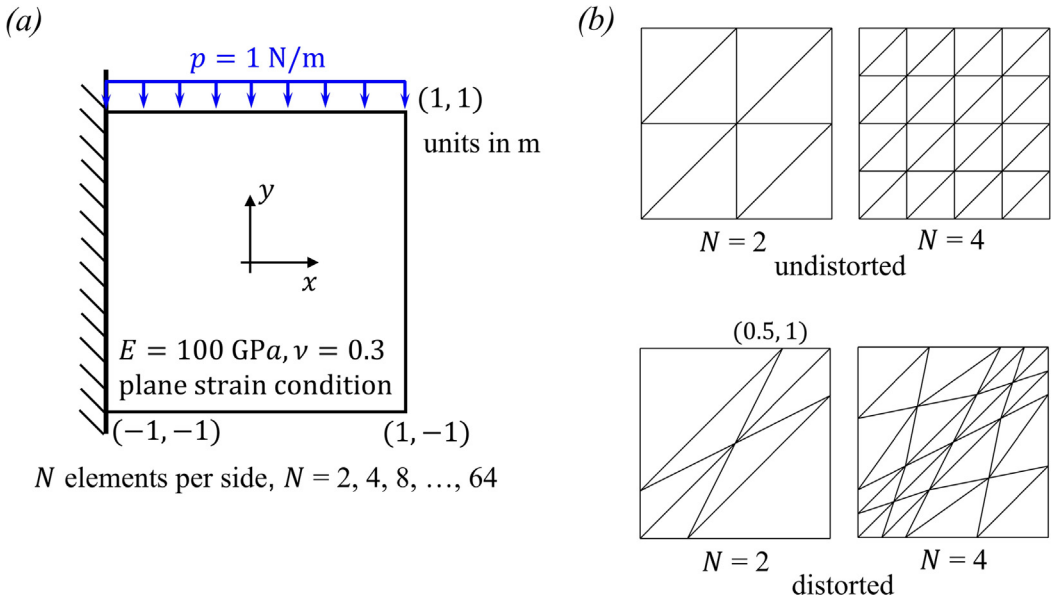

Fig. 7. Cantilever plate subjected to a surface traction; (a) Description of the problem; the plate is subjected to a uniformly distributed load $p = 1$ N/m; (b) Meshes used; the meshes are generated from the 4-node element meshes introduced in Fig. 4, by dividing a 4-node element into two 3-node elements.

2.2. Imposition of Dirichlet boundary conditions

We impose the Dirichlet (displacement) boundary conditions by using the appropriate nodal polynomials, similarly to enforcing the displacement boundary conditions in the traditional finite element method. For example, with a node K on a Dirichlet boundary, we will encounter two cases, see Fig. 2, where we impose the "zero displacement" boundary condition, on a two-dimensional analysis domain. When the node is located at a point of a smooth boundary as shown in Fig. 2a, we use the following nodal polynomial for node K to impose the displacement boundary condition.

$$u_K = a_{K1}\eta + a_{K2}\xi\eta + \text{higher} - \text{order terms} \tag{9}$$

where the ξ- and η-directions are tangential and perpendicular to the boundary, respectively.

In case the node is at a point of a non-smooth boundary, see Fig. 2b, we use

$$u_K = a_{K1}\xi\eta + \text{higher} - \text{order terms} \tag{10}$$

In addition, the natural (force) boundary conditions are weakly imposed as in traditional finite element analysis.

2.3. AMORE and coupling elements

The AMORE scheme discretizes the interior analysis domain with regular *undistorted* traditional elements and the domains near boundaries, that cannot be meshed with undistorted elements, with overlapping finite elements [1].

In order to have regular and overlapping elements in a discretization, we need to formulate elements that have both overlap-

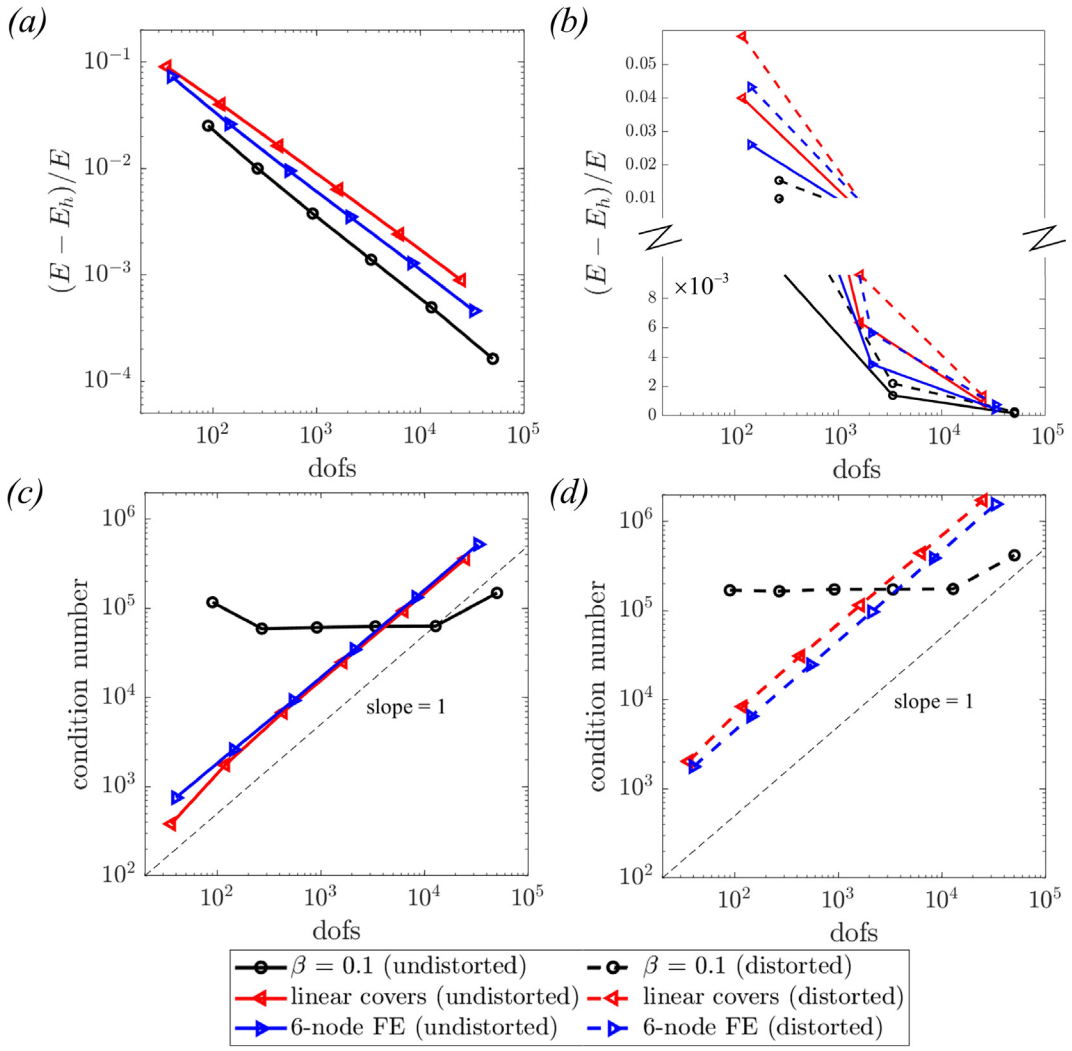

Fig. 8. Cantilever plate problem solved using the new 3-node triangular overlapping element with the quadratic basis, the traditional 6-node finite element, and the 3-node finite element with linear covers; (a) Convergence of strain energy using the undistorted meshes ($N = 2, 4, 8, \ldots, 64$); (b) Comparison between the strain energy errors obtained using the undistorted and distorted meshes ($N = 4$, 16, and 64); note that the y-axis uses the linear scale; (c) Change of condition number with refinement of the undistorted mesh; (d) Change of condition number with refinement of the distorted mesh.

ping and traditional element nodes. For such *coupling* elements, we construct ψ following the previously proposed method [1],

$$\psi_I = \begin{cases} \alpha & \text{for } I \in \Lambda_{FE} \\ \sum_{K\in\Lambda_{OFE}} \phi_K^I u_K + \sum_{K\in\Lambda_{FE}} \phi_K^I \alpha & \text{for } I \in \Lambda_{OFE} \end{cases} \tag{11}$$

with

$$\alpha = \sum_{K\in\Lambda_{OFE}} h_K a_{K1} + \sum_{K\in\Lambda_{FE}} h_K u_K \tag{12}$$

where Λ_{OFE} and Λ_{FE} are the sets of overlapping and traditional element nodes, respectively, and when the summation is over traditional finite element nodes (like in the last term) u_K is the nodal unknown of the traditional element node K.

3. Numerical aspects

The performance of the overlapping elements is based to a large degree on the stability of the discretizations and the accuracy reached in solutions. We first focus on the stability of the solution scheme and then briefly also on the convergence and expected accuracy of solutions.

The scheme is stable provided each element is stable (does not contain any spurious mode) [12]. In the following, we show that the overlapping elements pass the zero energy mode test when the numerical integration schemes suggested below are used.

3.1. Numerical integration and zero energy mode test

The matrices of each overlapping element are evaluated using the numerical integration schemes given in Table 1 [12].

The test inspects whether an unsupported element contains a spurious zero energy mode. By *unsupported* element we mean that all degrees of freedom (dofs) including all polynomial terms are free. If a single element has no spurious mode for the integration scheme used, a patch of elements will also not contain a spurious mode. We test the undistorted and geometrically distorted elements shown in Fig. 3. We use $E = 2 \times 10^9$ Pa, $\nu = 0.3$, and $\beta = 0.03$ for all elements, and the plane stress case is considered for two-dimensional elements.

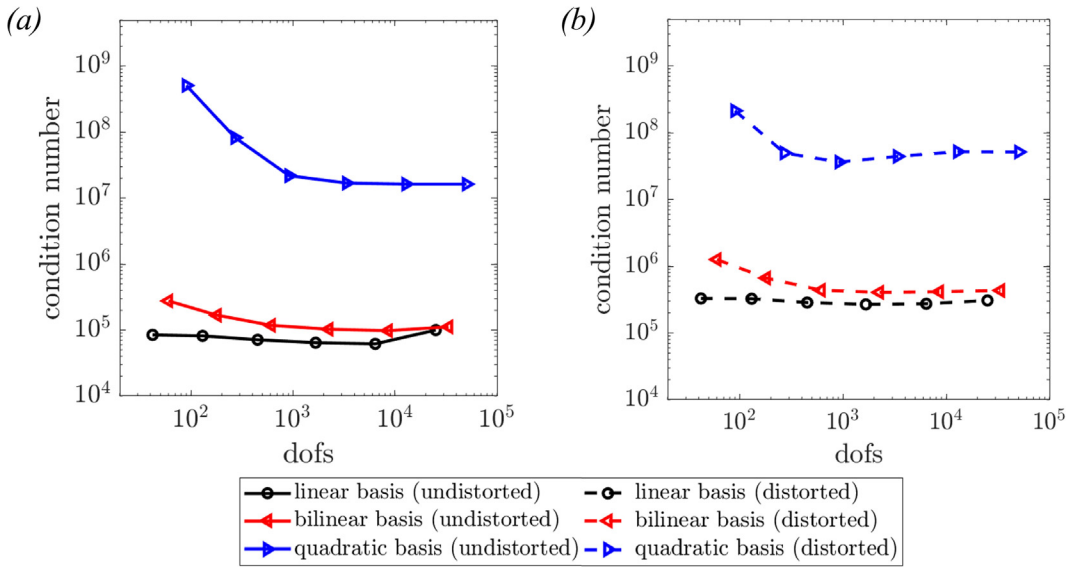

Fig. 9. Effect of the order of polynomial basis on the condition number; the new 3-node overlapping element with $\beta = 0.01$ is used for the undistorted and distorted meshes; (a) Change of condition number with refinement of the undistorted mesh; (b) Change of condition number with refinement of the distorted mesh.

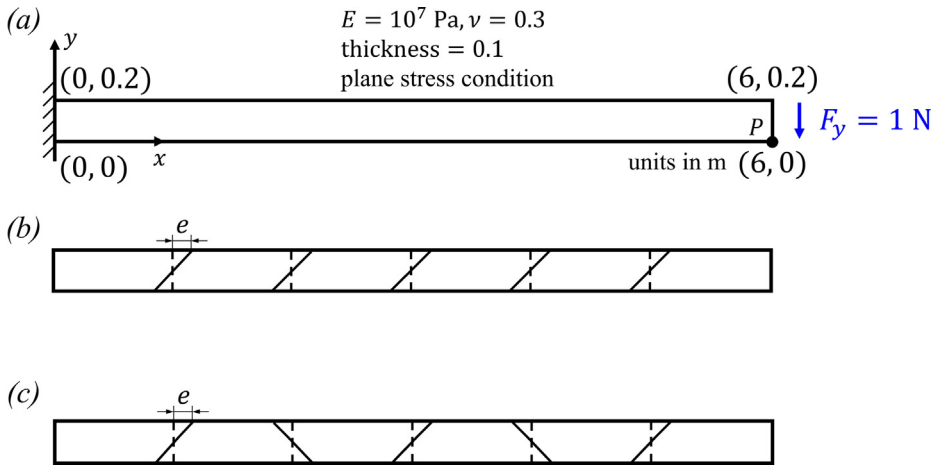

Fig. 10. Thin beam problem; (a) Description of the bending problem; total applied force is 1 N; (b) Parallelogram mesh used; (c) Trapezoidal mesh used.

Table 4
Normalized y-direction displacement at the tip ($x = 6$, $y = 0$); for the normalization the reference displacement is -0.1081 m.

9-Node FE (72 dofs)	$e = 0$ m	0.1	0.2	0.3	0.4
Parallelogram	0.9901	0.9813	0.9397	0.8770	0.8252
Trapezoidal	0.9901	0.9811	0.9234	0.8422	0.7966
4-Node OFE (156 dofs)	0	0.1	0.2	0.3	0.4
Parallelogram	0.9909	0.9917	0.9925	0.9920	0.9905
Trapezoidal	0.9909	0.9913	0.9910	0.9903	0.9906

Without a spurious mode, the two- and three-dimensional elements should have only three and six zero eigenvalues, respectively. These zero eigenvalues correspond to rigid body modes [12], where of course numerical round-off prevents to obtain exactly zero eigenvalues. As we see in Tables 2 and 3, the two-dimensional and three-dimensional elements pass the test. However, it is also seen that as the order of the polynomial basis we use increases, the lowest non-zero eigenvalue decreases. This decrease means in practice that the condition number of assembled stiffness matrices increases as the order of the element basis increases.

3.2. Positive definiteness of coefficient stiffness matrix

Since each overlapping element does not contain a spurious zero energy mode, the use of these elements in an arbitrary mesh

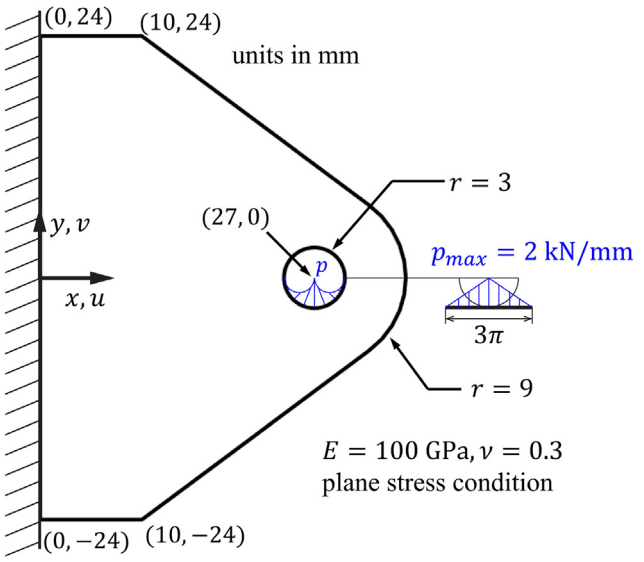

Fig. 11. Description of the bracket problem; the bracket is subject to the varying load p per unit length.

leads to a positive definite stiffness matrix, of course, provided proper displacement boundary conditions have been imposed. Hence the "linear dependency problem" in the governing equations observed in other generalized finite element methods is not present in a discretization using these overlapping finite elements. This is an important property of the discretization scheme.

Let us recall that, when using the finite element method with covers, even removing all cover degrees of freedom at the boundaries with prescribed displacements will not remove the instability for some elements, like for the 8-node brick element.

However, although a positive definite stiffness matrix is obtained using the elements of the above tables, we need to investigate whether this matrix is well-conditioned – in the same way as we also investigate the stiffness matrices of traditional and any new finite element formulations.

We solve in Sections 4 and 5 various problems using the overlapping finite elements and observe that in the numerical solutions of the problems considered, the new elements provide indeed quite well conditioned stiffness matrices on various meshes. We expected that the conditioning is acceptable and these solutions, although limited, are valuable.

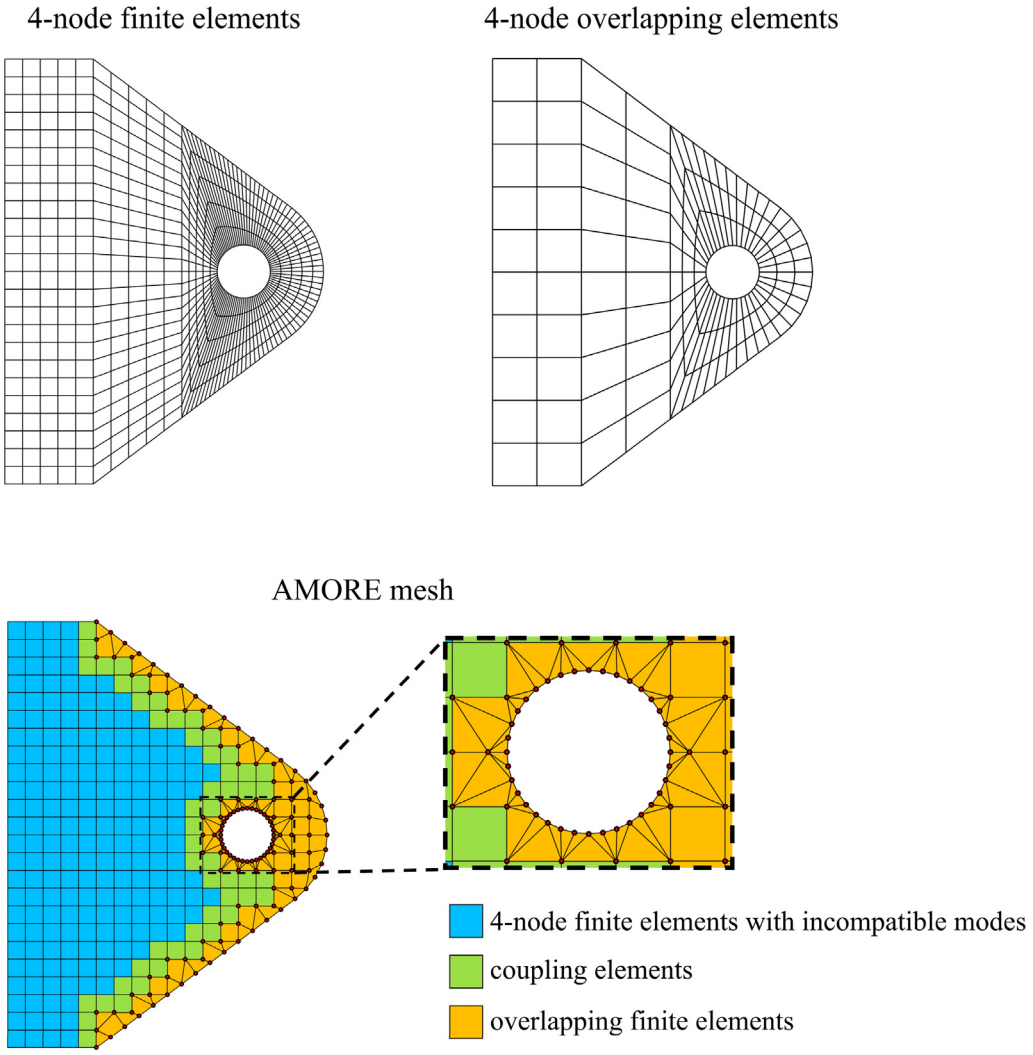

Fig. 12. Meshes used for the analysis of the bracket problem; the 4-node finite element mesh (1,602 dofs) is employed for two analyses, first using the 4-node compatible displacement-based finite element and then using the 4-node finite element with incompatible modes; both the 4-node overlapping element mesh (1,588 dofs) and AMORE mesh (1,560 dofs) use the bilinear basis and β = 0.03; an overlapping element node of the AMORE mesh is marked as a node.

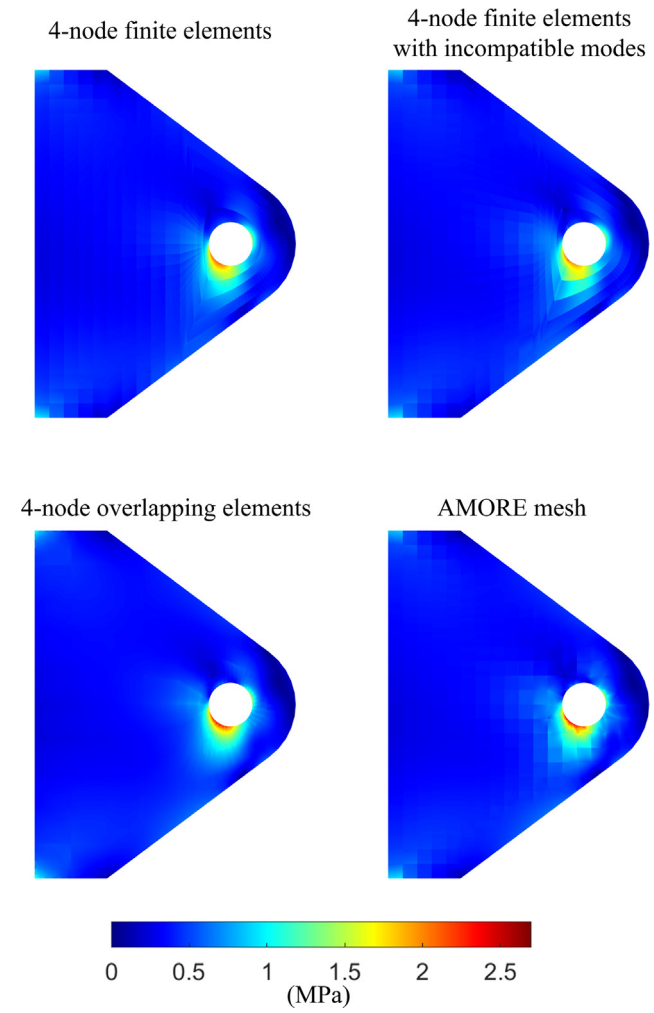

Fig. 13. von Mises stress distributions; the stress around the hole is underestimated when the mesh using the traditional elements is employed while it is well predicted when the 4-node OFE and AMORE meshes are used (see Table 5); also, the stress fields predicted using the OFE and AMORE meshes are smoother.

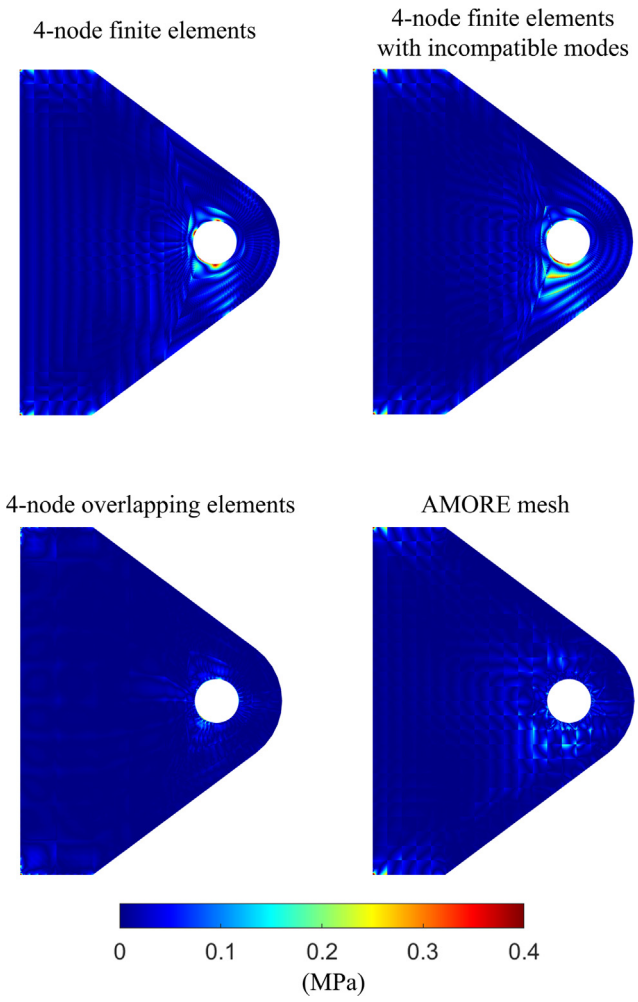

Fig. 14. Absolute error distributions of von Mises stress.

3.3. Distortion-insensitivity and convergence rates

A traditional geometrically distorted element may lose its polynomial completeness and hence predictive capability [25]. This loss deteriorates the solution accuracy, in particular when a coarse mesh is used, and rather coarse meshes are often utilized in practice [12]. We have shown that our proposed overlapping elements keep their polynomial completeness in reasonable distortions and thus have robust predictive capability. We show in Sections 4 and 5 that the new overlapping elements are also quite distortion-insensitive. For example, in Section 4.3, we observe that the 4-node overlapping element using the quadratic basis is less sensitive to distortion than the traditional 9-node element which also preserves its quadratic completeness when angularly distorted [12,25].

The distortion insensitivity also means that the convergence rates are little affected by element distortions. For example, when the p-th order polynomial basis is used, the formulation achieves $2p$-th order convergence of strain energy error [12], of course, when the problem solved has a sufficiently smooth solution [26]

$$E - E_h \leqslant c\, h^{2p} \tag{13}$$

where E and E_h are the strain energies of the exact and numerical solutions, respectively, h is the element size, and c is a constant. We find that the overlapping finite elements may also provide a small c which implies good accuracy. A small change in accuracy of the solution when the mesh is distorted must be expected because each element covers a different domain as it becomes distorted.

3.4. Effect of β on accuracy and conditioning

The magnitude of the parameter β affects the solution accuracy and the conditioning of the governing stiffness matrix. With $\beta \to 0$ we obtain the method of finite elements with interpolation covers which reproduces polynomial fields one order higher than the nodal polynomial used. Hence, as $\beta \to 0$ we obtain higher accuracy in a solution. However, at the same time, using $\beta \to 0$ renders the governing equations ill-conditioned because the finite element method with interpolation covers is not stable when the displacement boundary conditions are enforced using the scheme of Section 2.2. We confirm these observations in our numerical tests (see Sections 4.1 and 5.1). Given these element behaviors, it is desirable to use an optimal value of β for both good accuracy and a reasonable conditioning. Note that the described asymptotic behaviors are found for both cases, $\beta > 0$ and $\beta < 0$. However, we consider in this paper only the use of $\beta > 0$ since the use of $\beta < 0$ results in little difference of the numerical solutions.

Table 5
Numerical estimates for the bracket problem; the reference solutions for strain energy, maximum von Mises stress, maximum x-displacement ($u_{\max}$), and minimum y-displacement ($v_{\min}$) are 1.0439×10^{-3}N·m, 2.564 MPa, 5.230×10^{-5} mm, and -2.933×10^{-4} mm, respectively; all calculations shown in the table are normalized by the reference solution.

Mesh	Strain energy	Maximum von Mises stress	$u_{\max}$	$v_{\min}$
4-Node FE (1,602 dofs)	0.9867	0.8290	0.9784	0.9836
Incompatible (1,602 dofs)	0.9940	0.8721	0.9974	0.9929
4-Node OFE (1,588 dofs)	0.9961	0.9567	0.9912	0.9934
AMORE (1,560 dofs)	0.9933	1.0250	0.9947	0.9929

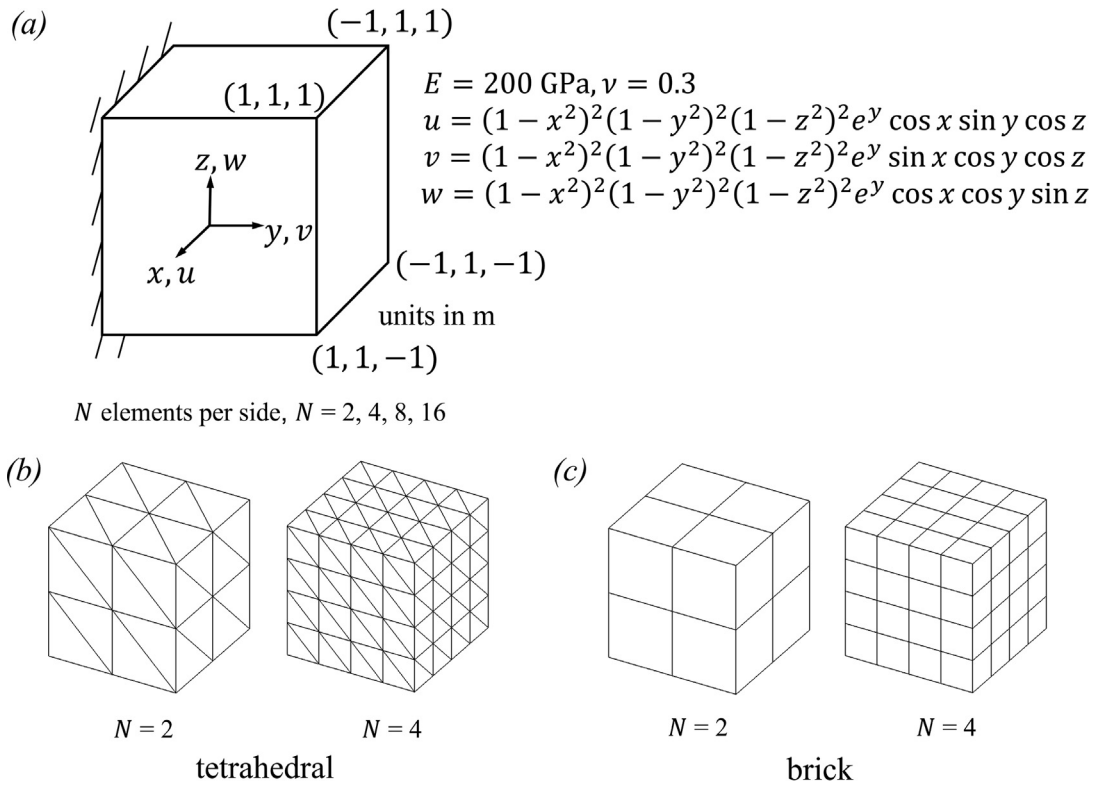

Fig. 15. Three-dimensional adhoc problem; (a) Description of the problem; (b) Meshes of tetrahedral elements; (c) Meshes of brick elements.

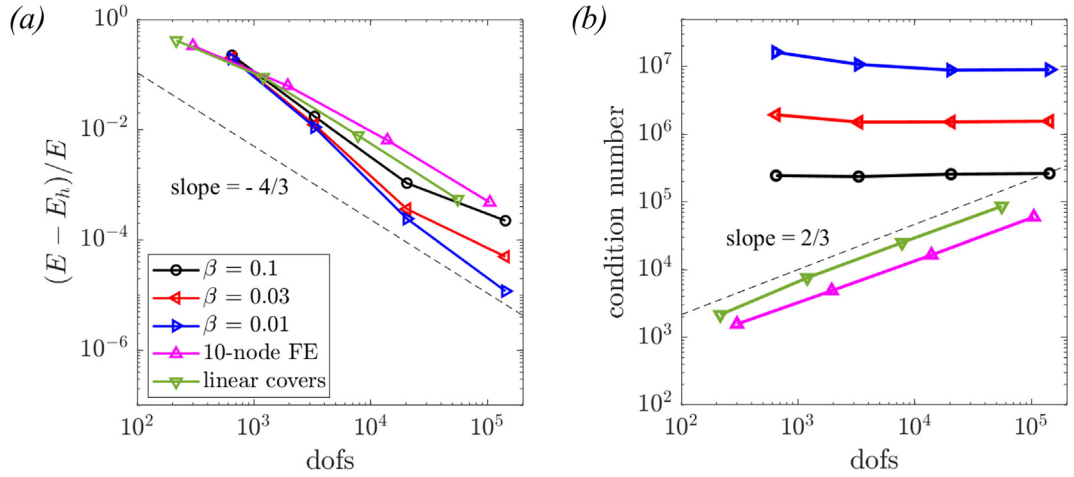

Fig. 16. Adhoc problem solved with the meshes of tetrahedral elements; (a) Convergence of strain energy; (b) Change of condition number with mesh refinement.

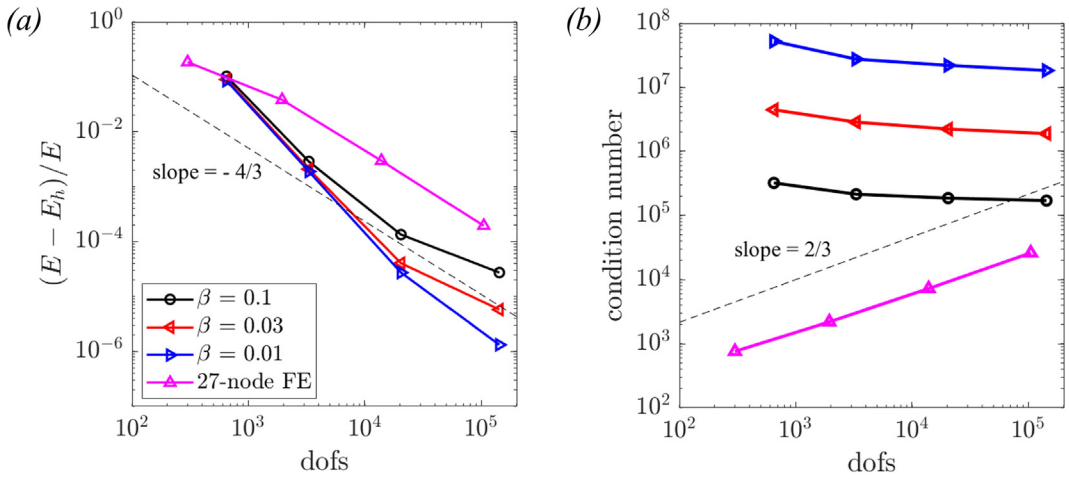

Fig. 17. Adhoc problem solved with the meshes of brick elements; (a) Convergence of strain energy; (b) Change of condition number with mesh refinement.

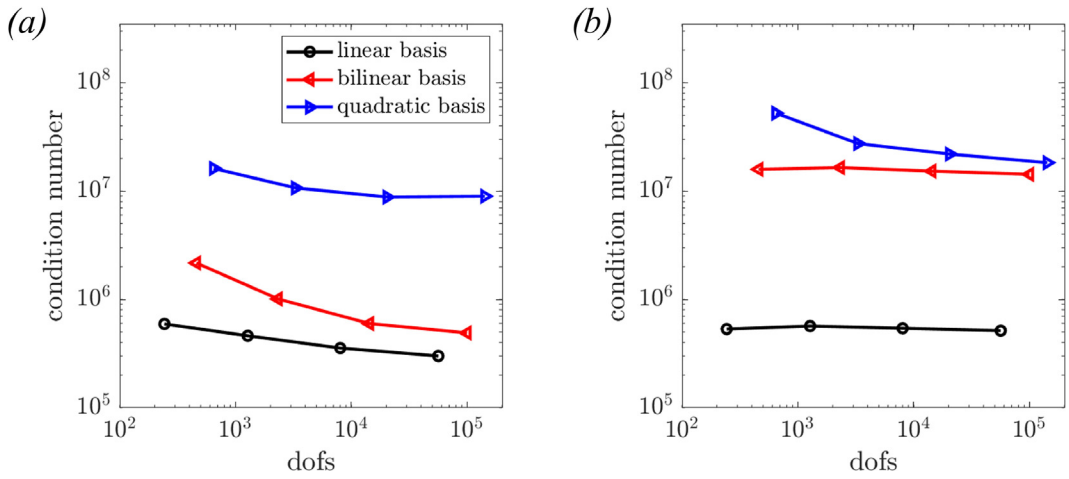

Fig. 18. Effect of the order of polynomial basis on the condition number; $\beta = 0.01$ is used; (a) Change of condition number with refinement of the new 4-node tetrahedral overlapping element mesh; (b) Change of condition number with refinement of the new 8-node brick overlapping element mesh.

4. Numerical tests of two-dimensional elements

In this section we solve several two-dimensional problems in linear statics to study the performance of the new 3-node triangular and 4-node quadrilateral overlapping elements. We focus on investigating the accuracy and conditioning of the new elements, comparing the results also to the results obtained when using their traditional finite element counterparts.

In the convergence curves we plot the strain energy errors versus the total number of degrees of freedom (dofs) because the dofs are a better measure in this study than using the element size h. Also, we use logarithmic measures unless otherwise indicated.

4.1. An adhoc problem

We first solve the two-dimensional adhoc problem illustrated in Fig. 4, see Ref. [19], using the new 4-node quadrilateral overlapping element with the quadratic polynomial basis. For the given displacement field, the body force is calculated and imposed. We use the solutions obtained with traditional 9-node elements for comparisons. The results are given in Fig. 5.

As expected, the new overlapping finite element gives the optimal convergence rate, and for a smaller β the overlapping element achieves higher accuracy, see Fig. 5a. For a given number of degrees of freedom, the overlapping finite element method provides better accuracy than the finite element method. The sensitivity to mesh distortion is illustrated in Fig. 5b, where we notice that the change in error introduced by mesh distortion is quite small when the overlapping finite element is used.

We also study the change of condition number with mesh refinement. The condition number is defined as the ratio of the largest to the smallest eigenvalues of the stiffness matrix. As shown in Fig. 5c and d, the use of the new 4-node overlapping element results in a reasonably conditioned stiffness matrix, but the condition number increases as β decreases. Also, to some degree, the condition numbers of the overlapping element models initially decrease with mesh refinement and then stay almost constant in further refinements.

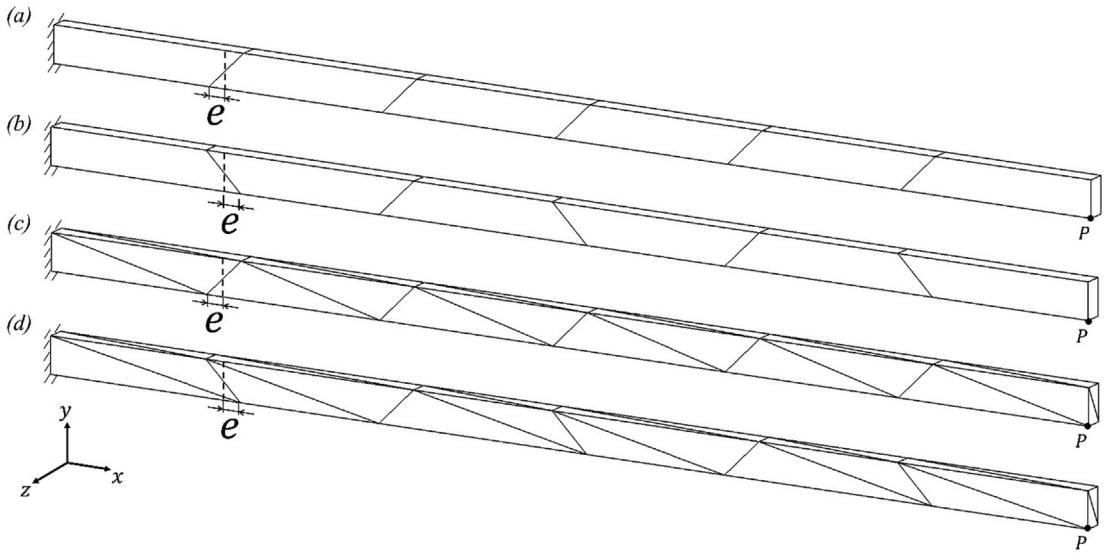

Fig. 19. Three-dimensional meshes used for solving the problem of Section 4.3; (a) Parallelogram mesh using brick elements; (b) Trapezoidal mesh using brick elements; (c) Parallelogram mesh using tetrahedral elements; (d) Trapezoidal mesh using tetrahedral elements.

Table 6
Normalized y-direction displacement calculated by the new overlapping finite element method; $\beta = 0.03$ is used.

4-Node OFE (768 dofs)	$e = 0$ m	0.1	0.2	0.3	0.4
Parallelogram	0.9747	0.9729	0.9692	0.9647	0.9603
Trapezoidal	0.9747	0.9705	0.9635	0.9554	0.9444
8-Node OFE (768 dofs)	0	0.1	0.2	0.3	0.4
Parallelogram	0.9841	0.9837	0.9831	0.9821	0.9806
Trapezoidal	0.9841	0.9834	0.9822	0.9812	0.9805

Table 7
Normalized y-direction displacement calculated by the new overlapping finite element method; $\beta = 0.01$ is used.

4-Node OFE (768 dofs)	$e = 0$ m	0.1	0.2	0.3	0.4
Parallelogram	0.9807	0.9810	0.9808	0.9800	0.9791
Trapezoidal	0.9807	0.9797	0.9782	0.9759	0.9728
8-Node OFE (768 dofs)	0	0.1	0.2	0.3	0.4
Parallelogram	0.9876	0.9877	0.9879	0.9878	0.9876
Trapezoidal	0.9876	0.9876	0.9875	0.9873	0.9872

Table 8
Normalized y-direction displacement calculated by the finite element method using the traditional 27-Node element; the $6 \times 1 \times 1$ mesh is the mesh given in Fig. 19a or b, and the $12 \times 2 \times 2$ mesh is obtained by splitting the element edges of the $6 \times 1 \times 1$ mesh in half and generating eight elements from an element.

27-Node FE $6 \times 1 \times 1$ mesh (324 dofs)	$e = 0$ m	0.1	0.2	0.3	0.4
Parallelogram	0.9784	0.9690	0.9267	0.8659	0.8169
Trapezoidal	0.9784	0.9682	0.9077	0.8296	0.7883
27-Node FE $12 \times 2 \times 2$ mesh (1,800 dofs)	0	0.1	0.2	0.3	0.4
Parallelogram	0.9907	0.9895	0.9848	0.9745	0.9551
Trapezoidal	0.9907	0.9900	0.9884	0.9872	0.9861

Additionally, we show in Fig. 6 that the use of a higher order nodal basis leads to an increase of the condition number. We expected this increase as mentioned in Section 3 where we noticed that the use of a higher order polynomial basis results in a smaller first nonzero eigenvalue in the element mode test.

4.2. A cantilever plate subjected to an in-plane surface traction

Next we solve the plane strain problem shown in Fig. 7, see Ref. [10], using the new 3-node triangular overlapping element with the quadratic polynomial basis. We consider also the traditional

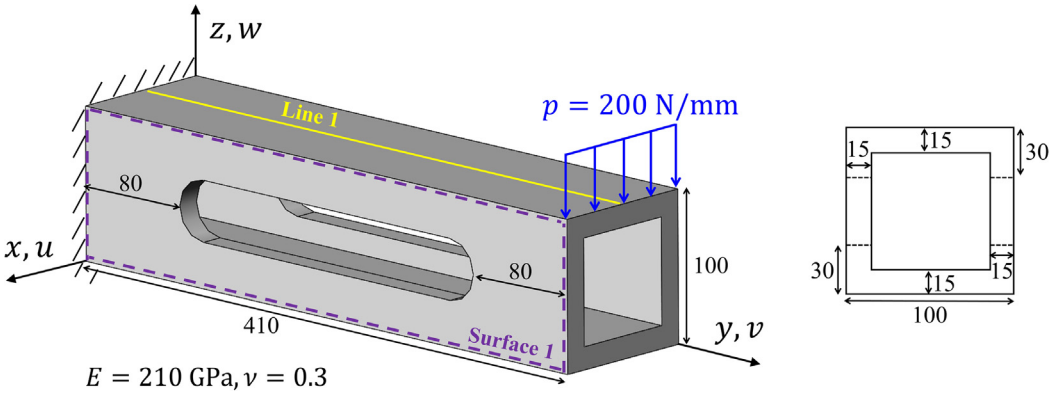

Fig. 20. Description of machine tool jig problem; a uniformly distributed load p per unit length is applied, lengths in mm.

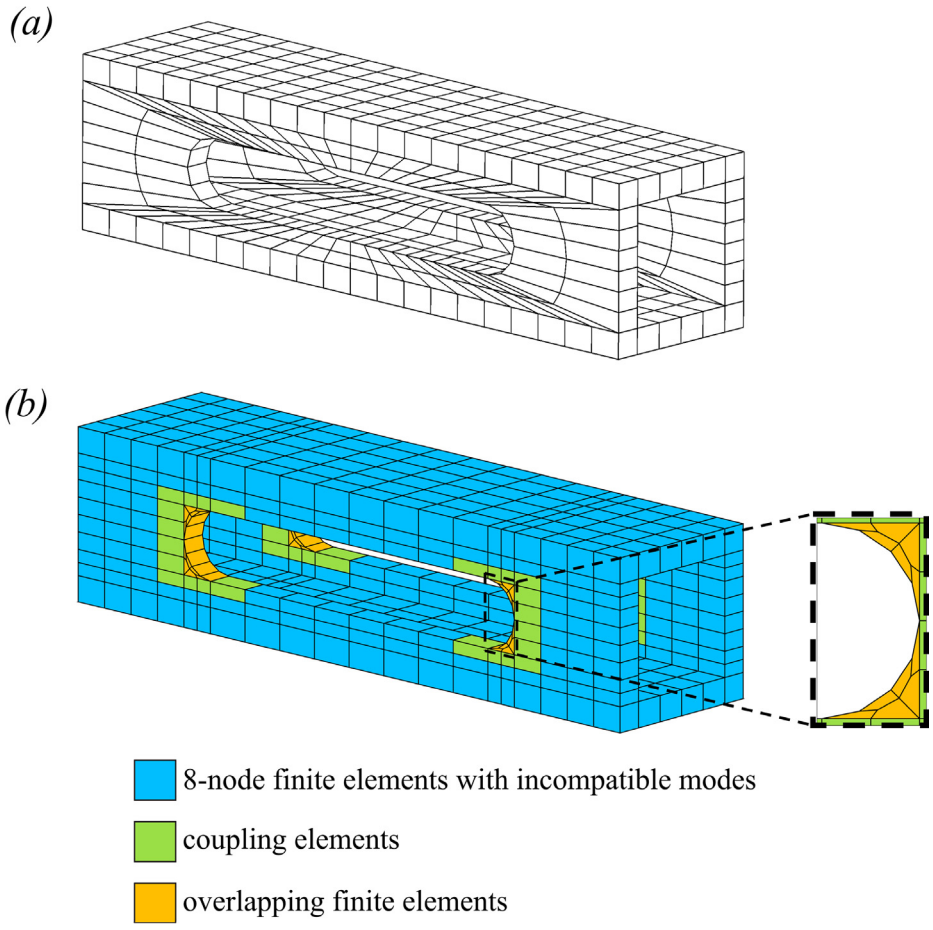

Fig. 21. Meshes used for solving the machine tool jig problem; (a) Traditional mesh using the 8-node brick element with incompatible modes (2,988 dofs); (b) AMORE mesh (4,764 dofs); the overlapping element nodes use the linear polynomial basis and $\beta = 0.01$.

6-node finite element and the 3-node finite element with linear covers [19]. As in the previous example, we study the accuracy, conditioning, and sensitivity to mesh distortion of the element. The reference solution is obtained using a mesh of 256×256 traditional 9-node finite elements. The results are provided in Fig. 8.

For a given number of dofs, the use of the new 3-node overlapping element provides better accuracy than both the traditional 6-node element and the 3-node finite element with linear covers. We only present results using the overlapping finite element with $\beta = 0.1$ since the use of other values of β provides almost the same solution accuracy in this problem. Considering the distortion-sensitivity of the elements, we notice that the new 3-node overlapping element is less sensitive to mesh distortions.

The condition numbers using the new 3-node overlapping finite element method are reasonable and the trend in values with mesh refinement is similar to that observed in the use of the new 4-node overlapping element.

Also, as expected, the use of a higher order nodal basis leads to an increased condition number, see Fig. 9.

4.3. Thin beam problem

The thin beam problem considered here, see Fig. 10, has been used in various studies to see the effect of mesh distortion on the predictive capability of an element [1,11,15,27]. We use the dimension e to represent the degree of distortion and compare the solution accuracies when using the new 4-node overlapping finite element and the traditional 9-node element. The 4-node overlapping element uses the quadratic polynomial basis and $\beta = 0.03$.

We solve for the y-direction displacement of the tip at point P given by ($x = 6$, $y = 0$). As can be seen in Table 4, the use of the 4-node overlapping element provides a more accurate solution than using the 9-node element. In particular, the solutions using the overlapping element are uniformly accurate with the same small error regardless of the magnitude of e which does not hold when using the 9-node element.

4.4. Bracket problem and AMORE scheme

Finally, we solve the bracket problem shown in Fig. 11 to study the accuracy of the new overlapping finite element in the AMORE scheme. As shown in Fig. 12, the problem is solved four times, namely using: a mesh of 4-node compatible displacement-based finite elements, the same mesh but of 4-node elements with incompatible modes [12], a mesh of 4-node overlapping elements, and finally an AMORE mesh. We use the bilinear polynomial basis and $\beta = 0.03$ for the overlapping element and AMORE meshes. For use of AMORE the non-overlapping 4-node elements contain the incompatible modes, with the coupling elements not carrying these modes. In order to compare the predictive capabilities we have selected the meshes to correspond to almost identical numbers of degrees of freedom. The reference solution is obtained using a very fine mesh of 9-node elements with 116,238 dofs.

The calculated von Mises stress distributions and absolute errors are shown in Figs. 13 and 14, respectively. The 4-node overlapping element and the AMORE scheme provide more accurate stress fields than the meshes of traditional 4-node elements and 4-node elements with incompatible modes. Further results are listed in Table 5 showing that the maximum von Mises stress is substantially underestimated when the mesh using the traditional displacement-based element or incompatible modes element is used whereas the stress is well predicted when the overlapping element and AMORE meshes are employed.

5. Numerical tests of three-dimensional elements

In this section, we solve linear static three-dimensional problems to study the accuracy and conditioning of the new 4-node tetrahedral and 8-node brick overlapping elements. We also consider the traditional finite elements for comparison.

5.1. An adhoc problem

We study the accuracy and conditioning of the new 4-node tetrahedral and 8-node brick overlapping elements in the solution of the adhoc problem shown in Fig. 15, see Ref. [16]. For the given displacement field, the body force is calculated and imposed.

The results are presented as in the studies of Section 4.

First, we test the new 4-node tetrahedral overlapping element using the quadratic polynomial basis with the meshes described in Fig. 15b. Meshes using traditional 10-node elements and 4-node elements enriched by linear covers [19,20] are also considered. As shown in Fig. 16a, the use of the 4-node overlapping element provides better accuracy than the other elements for about the same number of degrees of freedom used. The solutions using the 4-node overlapping element show the optimal convergence rate as predicted by theory [11,26]. As in the two-dimensional adhoc problem, the use of a smaller β results in higher accuracy. The condition number of the stiffness matrix is also examined, see Fig. 16b. A smaller β results in a higher condition number, but the condition numbers are reasonable. Also, the numbers remain almost constant for the tested range of degrees of freedom.

The new 8-node brick overlapping element with the quadratic basis is also tested with the meshes shown in Fig. 15c. The results are given in Fig. 17. The use of the new 8-node overlapping element provides better accuracy than traditional 27-node elements for a given number of degrees of freedom. The trend of the condition number with mesh refinement, see Fig. 17b, is the same as that from the use of the new 4-node tetrahedral overlapping element.

The effect of the order of the polynomial basis on the condition number is further studied with refinement of the meshes, see Fig. 18. As expected, for both the new tetrahedral and brick overlapping elements, an increase of the order of the basis leads to an increase of the condition number.

5.2. Slender beam problem

We solve the problem used in Section 4.3 now in three dimensions. The new 4-node tetrahedral and 8-node brick overlapping elements with the quadratic basis are tested using the meshes in Fig. 19. For comparison, we also solve the problem using traditional 27-node brick finite elements. The y-direction displacement at the tip point P is predicted, and the reference displacement is -0.1081 m.

Tables 6 and 7 give the displacement predictions when β is equal to 0.03 and 0.01, respectively. Overall, the use of the 4-node and 8-node overlapping elements gives accurate predictions, which are quite insensitive to mesh distortions. The use of a smaller β gives more accurate solutions and shows even less sensitivity to the mesh distortions. For comparison, Table 8 gives the results using the 27-node element.

5.3. Machine tool jig problem

To further study the effectiveness of the new overlapping elements and the AMORE scheme, we solve the three-dimensional problem shown in Fig. 20, see Ref. [28]. We use the traditional and AMORE meshes shown in Fig. 21 and compare the predictive capabilities. The traditional mesh uses the traditional 8-node finite element with incompatible modes. The AMORE mesh consists of 8-node brick element with incompatible modes, 8-node displacement-based coupling elements, and 8-node overlapping elements. The coupling element is formulated as in Section 2.3. All overlapping element nodes use the linear polynomial basis and $\beta = 0.01$. The reference solution is obtained using a very fine mesh of 27-node finite elements of 717,282 dofs.

The normalized strain energies obtained with the traditional and AMORE meshes are 0.9561 and 0.9559, respectively, with the reference strain energy = 10.34 N·m. Along Line 1 (see Fig. 20), the z-direction displacement and normal stress in the y direction are evaluated. As can be seen in Fig. 22, both analyses give reasonable predictions. We also examine the von Mises stress distribution on Surface 1 (see Fig. 20). The stress distributions and the absolute error are given in Figs. 23 and 24, respectively. The solution using the AMORE mesh provides better stress predictions, particularly in the regions of stress concentrations.

While we give in Fig. 21 the total number of degrees of freedom used for the meshes, we do not report any solution times, since for such comparison an effective sparse solver would need to be

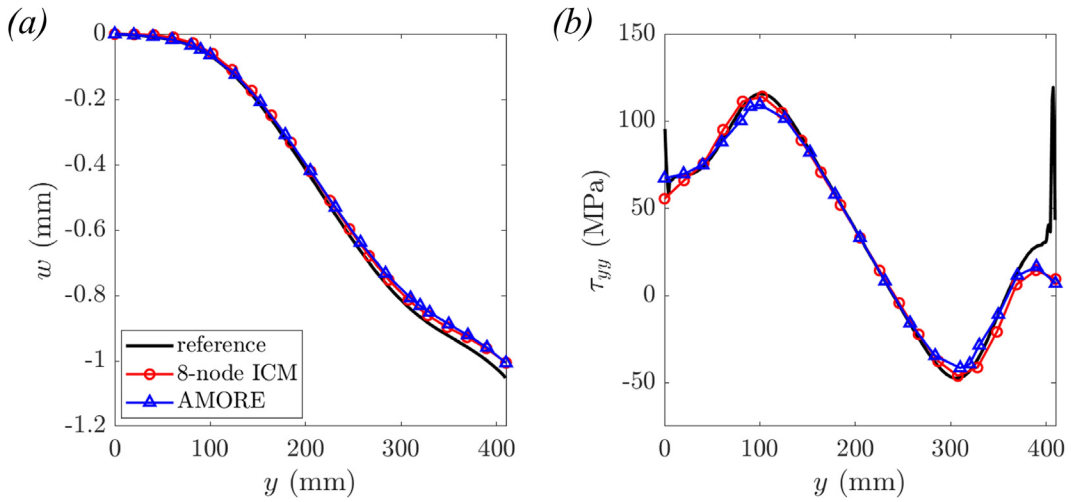

Fig. 22. Numerical results for the machine tool jig problem along Line 1 shown in Fig. 20; the 8-node ICM label corresponds to the 8-node brick element with incompatible modes; (a) z-direction displacement; (b) normal stress in the y direction (averaged at nodes).

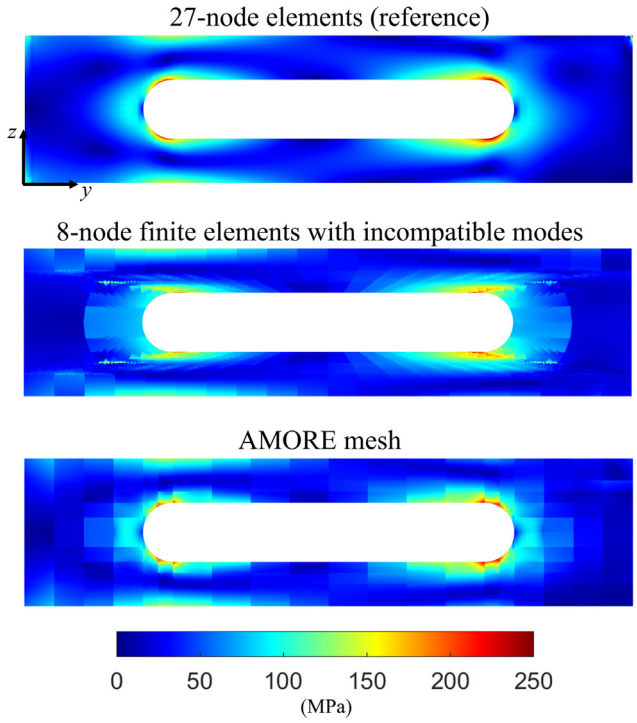

Fig. 23. von Mises stress distributions on Surface 1.

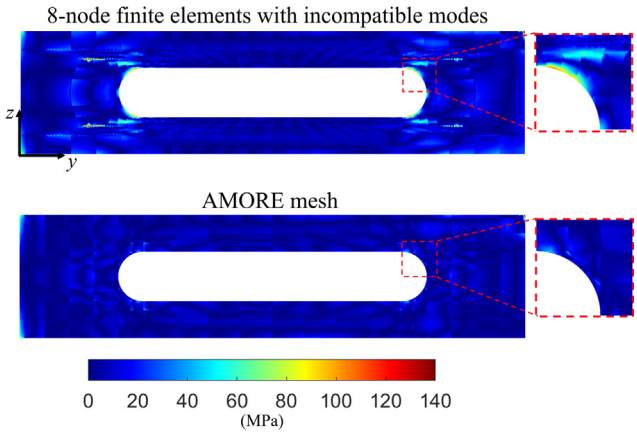

Fig. 24. Absolute error distributions of von Mises stress on Surface 1.

employed. The solutions given here have been obtained with a relatively simple MATLAB code.

6. Concluding remarks

We have presented two- and three-dimensional overlapping elements with enhancements that we consider valuable for the general analyses of solids.

Firstly, the elements are formulated without an "explicit" function to be interpolated, hence no radii as for the method of finite spheres [2] and the earlier proposed overlapping elements are used [9]. However, a parameter β is employed which implicitly means that a function is interpolated. This way to proceed is more direct and simpler, and we have obtained good results when the value of β is set to be constant (=0.01) throughout all solutions.

Secondly, the elements show stability and resulted in reasonable condition numbers in the solutions we presented. As mentioned in the paper, generalizing or enriching finite element discretizations can introduce a linear dependency of the governing equations. This linear dependency has been addressed by various but not satisfactory schemes. Our formulation of the overlapping finite elements gives always a positive definite stiffness matrix, as long as $\beta \neq 0$, and reasonable condition numbers which however increase as β decreases. This increase is expected since when $\beta = 0$ the overlapping elements are elements with interpolation covers.

We have discussed and illustrated the above observations in the solutions of various two- and three-dimensional problems and also when using the AMORE scheme. These experiences show that the enhancements are valuable and provide further evidence of the usefulness of overlapping finite elements.

However, many more studies are needed. These pertain to various areas relating to the overlapping finite elements and the AMORE scheme. For example, the solution times should be studied using an effective implementation of the solution methods, and the further development of the schemes in frequency solutions, transient analyses, and general nonlinear analyses need to be pursued.

Furthermore, for an effective use of AMORE, efficient AMORE meshing procedures for two- and three-dimensional geometries need to be developed, such that the meshing effort in AMORE is much smaller than in traditional finite element meshing when complex geometries are considered. In fact, it is the premise to render the AMORE scheme attractive by meshing the bulk volume of a complex three-dimensional geometry with, for example, undistorted brick elements (that give a coarse grid and are computationally effective to generate) and the rest of the total geometry with overlapping tetrahedral elements that can be highly distorted [1,7]. Although the number of equations to be solved for the AMORE model will then be in many cases larger than for the traditional model (to reach the same solution accuracy), since the time for meshing is much less, the total time spent on the analysis is much reduced.

Declaration of Competing Interest

The authors declare that they have no known competing financial interests or personal relationships that could have appeared to influence the work reported in this paper.

Appendix A. Nodal values for the interpolation of ϕ_K^I

In the new OFE formulation, as in our prior works, the function ϕ_K^I is interpolated using a traditional higher order finite element that has mid-side nodes. We present below the nodal values for the interpolation of ϕ_K^I. Here, $A = 0.5 - \beta$, $B = 0.5 + \beta$, and an empty cell represents the value of zero. The node numbering is given in Fig. A1 (see Tables A1–A5). We note that always $\sum_{K=1}^{N} \phi_K^I = 1$.

Appendix B. Derivation of nodal values for the interpolation of ϕ_K^I and Eq. (6)

We do not explicitly interpolate a function to construct ϕ_K^I, but it is worth noting that ϕ_K^I can be obtained by interpolating a function and such function is not unique. For example, we can obtain the nodal values in Appendix A by assuming that we interpolate the following function over an element

$$\Phi_K^I = \frac{W_K^I}{\sum_{J\in\mathcal{N}} W_J^I}$$
$$W_J^I = \begin{cases} \gamma\, h_J(x)^2 & \text{for } I = J \\ h_J(x) & \text{for } I \neq J \end{cases} \tag{B.1}$$

where $\mathcal{N}$ is the index set of nodes of the element, γ is a free parameter, and $h_J(\boldsymbol{x})$ is the low order finite element function. Considering the 3-node triangular overlapping element, we derive some nodal values to demonstrate that the interpolation of Φ_K^I results in ϕ_K^I

Table A1
Fictitious nodal values for the interpolation of ϕ_K^I of the 3-node triangular element.

Nodes	i = 1	2	3	4	5	6
$\hat{\phi}_{1i}^1$	1			A		A
$\hat{\phi}_{2i}^1$		1		B	0.5	
$\hat{\phi}_{3i}^1$			1		0.5	B
$\hat{\phi}_{1i}^2$	1			B		0.5
$\hat{\phi}_{2i}^2$		1		A	A	
$\hat{\phi}_{3i}^2$			1		B	0.5
$\hat{\phi}_{1i}^3$	1			0.5		B
$\hat{\phi}_{2i}^3$		1		0.5	B	
$\hat{\phi}_{3i}^3$			1		A	A

Table A2
Fictitious nodal values for the interpolation of ϕ_K^I of the 4-node quadrilateral element.

Nodes	i = 1	2	3	4	5	6	7	8
$\hat{\phi}_{1i}^1$	1				A			A
$\hat{\phi}_{2i}^1$		1			B	0.5		
$\hat{\phi}_{3i}^1$			1			0.5	0.5	
$\hat{\phi}_{4i}^1$				1			0.5	B
$\hat{\phi}_{1i}^2$	1				B			0.5
$\hat{\phi}_{2i}^2$		1			A	A		
$\hat{\phi}_{3i}^2$			1			B	0.5	
$\hat{\phi}_{4i}^2$				1			0.5	0.5
$\hat{\phi}_{1i}^3$	1				0.5			0.5
$\hat{\phi}_{2i}^3$		1			0.5	B		
$\hat{\phi}_{3i}^3$			1			A	A	
$\hat{\phi}_{4i}^3$				1			B	0.5
$\hat{\phi}_{1i}^4$	1				0.5			B
$\hat{\phi}_{2i}^4$		1			0.5	0.5		
$\hat{\phi}_{3i}^4$			1			0.5	B	
$\hat{\phi}_{4i}^4$				1			A	A

Table A3
Fictitious nodal values for the interpolation of ϕ_K^I of the 4-node tetrahedral element.

Nodes	$i=1$	2	3	4	5	6	7	8	9	10
$\hat{\phi}_{1i}^1$	1				A		A	A		
$\hat{\phi}_{2i}^1$		1			B	0.5			0.5	
$\hat{\phi}_{3i}^1$			1			0.5	B			0.5
$\hat{\phi}_{4i}^1$				1				B	0.5	0.5
$\hat{\phi}_{1i}^2$	1				B		0.5	0.5		
$\hat{\phi}_{2i}^2$		1			A	A			A	
$\hat{\phi}_{3i}^2$			1			B	0.5			0.5
$\hat{\phi}_{4i}^2$				1				0.5	B	0.5
$\hat{\phi}_{1i}^3$	1				0.5		B	0.5		
$\hat{\phi}_{2i}^3$		1			0.5	B			0.5	
$\hat{\phi}_{3i}^3$			1			A	A			A
$\hat{\phi}_{4i}^3$				1				0.5	0.5	B
$\hat{\phi}_{1i}^4$	1				0.5		0.5	B		
$\hat{\phi}_{2i}^4$		1			0.5	0.5			B	
$\hat{\phi}_{3i}^4$			1			0.5	0.5			B
$\hat{\phi}_{4i}^4$				1				A	A	A

Table A4
Fictitious nodal values for the interpolation of ϕ_K^I of the 8-node brick element ($I=1, 2, 3, 4$).

Nodes	$i=1$	2	3	4	5	6	7	8	9	10	11	12	13	14	15	16	17	18	19	20
$\hat{\phi}_{1i}^1$	1								A			A					A			
$\hat{\phi}_{2i}^1$		1							B	0.5								0.5		
$\hat{\phi}_{3i}^1$			1							0.5	0.5								0.5	
$\hat{\phi}_{4i}^1$				1							0.5	B								0.5
$\hat{\phi}_{5i}^1$					1								0.5			0.5	B			
$\hat{\phi}_{6i}^1$						1							0.5	0.5				0.5		
$\hat{\phi}_{7i}^1$							1							0.5	0.5				0.5	
$\hat{\phi}_{8i}^1$								1							0.5	0.5				0.5
$\hat{\phi}_{1i}^2$	1								B			0.5					0.5			
$\hat{\phi}_{2i}^2$		1							A	A								A		
$\hat{\phi}_{3i}^2$			1							B	0.5								0.5	
$\hat{\phi}_{4i}^2$				1							0.5	0.5								0.5
$\hat{\phi}_{5i}^2$					1								0.5			0.5	0.5			
$\hat{\phi}_{6i}^2$						1							0.5	0.5				B		
$\hat{\phi}_{7i}^2$							1							0.5	0.5				0.5	
$\hat{\phi}_{8i}^2$								1							0.5	0.5				0.5
$\hat{\phi}_{1i}^3$	1								0.5			0.5					0.5			
$\hat{\phi}_{2i}^3$		1							0.5	B								0.5		
$\hat{\phi}_{3i}^3$			1							A	A								A	
$\hat{\phi}_{4i}^3$				1							B	0.5								0.5
$\hat{\phi}_{5i}^3$					1								0.5			0.5	0.5			
$\hat{\phi}_{6i}^3$						1							0.5	0.5				0.5		
$\hat{\phi}_{7i}^3$							1							0.5	0.5				B	
$\hat{\phi}_{8i}^3$								1							0.5	0.5				0.5
$\hat{\phi}_{1i}^4$	1								0.5			B					0.5			
$\hat{\phi}_{2i}^4$		1							0.5	0.5								0.5		
$\hat{\phi}_{3i}^4$			1							0.5	B								0.5	
$\hat{\phi}_{4i}^4$				1							A	A								A
$\hat{\phi}_{5i}^4$					1								0.5			0.5	0.5			
$\hat{\phi}_{6i}^4$						1							0.5	0.5				0.5		
$\hat{\phi}_{7i}^4$							1							0.5	0.5				0.5	
$\hat{\phi}_{8i}^4$								1							0.5	0.5				B

Table A5
Fictitious nodal values for the interpolation of ϕ_K^I of the 8-node brick element (I = 5, 6, 7, 8).

Nodes	$i=1$	2	3	4	5	6	7	8	9	10	11	12	13	14	15	16	17	18	19	20
$\hat{\phi}_{1i}^5$	1								0.5			0.5					B			
$\hat{\phi}_{2i}^5$		1							0.5	0.5								0.5		
$\hat{\phi}_{3i}^5$			1							0.5	0.5								0.5	
$\hat{\phi}_{4i}^5$				1							0.5	0.5								0.5
$\hat{\phi}_{5i}^5$					1								A			A	A			
$\hat{\phi}_{6i}^5$						1							B	0.5				0.5		
$\hat{\phi}_{7i}^5$							1							0.5	0.5				0.5	
$\hat{\phi}_{8i}^5$								1							0.5	B				0.5
$\hat{\phi}_{1i}^6$	1								0.5			0.5					0.5			
$\hat{\phi}_{2i}^6$		1							0.5	0.5								B		
$\hat{\phi}_{3i}^6$			1							0.5	0.5								0.5	
$\hat{\phi}_{4i}^6$				1							0.5	0.5								0.5
$\hat{\phi}_{5i}^6$					1								B			0.5	0.5			
$\hat{\phi}_{6i}^6$						1							A	A				A		
$\hat{\phi}_{7i}^6$							1							B	0.5				0.5	
$\hat{\phi}_{8i}^6$								1							0.5	0.5				0.5
$\hat{\phi}_{1i}^7$	1								0.5			0.5					0.5			
$\hat{\phi}_{2i}^7$		1							0.5	0.5								0.5		
$\hat{\phi}_{3i}^7$			1							0.5	0.5								B	
$\hat{\phi}_{4i}^7$				1							0.5	0.5								0.5
$\hat{\phi}_{5i}^7$					1								0.5			0.5	0.5			
$\hat{\phi}_{6i}^7$						1							0.5	B				0.5		
$\hat{\phi}_{7i}^7$							1							A	A				A	
$\hat{\phi}_{8i}^7$								1							B	0.5				0.5
$\hat{\phi}_{1i}^8$	1								0.5			0.5					0.5			
$\hat{\phi}_{2i}^8$		1							0.5	0.5								0.5		
$\hat{\phi}_{3i}^8$			1							0.5	0.5								0.5	
$\hat{\phi}_{4i}^8$				1							0.5	0.5								B
$\hat{\phi}_{5i}^8$					1								0.5			B	0.5			
$\hat{\phi}_{6i}^8$						1							0.5	0.5				0.5		
$\hat{\phi}_{7i}^8$							1							0.5	B				0.5	
$\hat{\phi}_{8i}^8$								1							A	A				A

$$\hat{\phi}_{11}^1 = \Phi_1^1(\boldsymbol{x}_1) = \frac{\gamma h_1(\boldsymbol{x}_1)^2}{\gamma h_1(\boldsymbol{x}_1)^2 + h_2(\boldsymbol{x}_1) + h_3(\boldsymbol{x}_1)} = \frac{\gamma}{\gamma+0+0} = 1$$
$$\hat{\phi}_{14}^1 = \Phi_1^1(\boldsymbol{x}_4) = \frac{\gamma h_1(\boldsymbol{x}_4)^2}{\gamma h_1(\boldsymbol{x}_4)^2 + h_2(\boldsymbol{x}_4) + h_3(\boldsymbol{x}_4)} = \frac{0.25\gamma}{0.25\gamma+0.5+0} = 0.5 - \frac{2-\gamma}{2(2+\gamma)}$$
$$\hat{\phi}_{24}^1 = \Phi_2^1(\boldsymbol{x}_4) = \frac{h_2(\boldsymbol{x}_4)}{\gamma h_1(\boldsymbol{x}_4)^2 + h_2(\boldsymbol{x}_4) + h_3(\boldsymbol{x}_4)} = \frac{0.5}{0.25\gamma+0.5+0} = 0.5 + \frac{2-\gamma}{2(2+\gamma)} \tag{B.2}$$
$$\hat{\phi}_{25}^1 = \Phi_2^1(\boldsymbol{x}_5) = \frac{h_2(\boldsymbol{x}_5)}{\gamma h_1(\boldsymbol{x}_5)^2 + h_2(\boldsymbol{x}_5) + h_3(\boldsymbol{x}_5)} = \frac{0.5}{0+0.5+0.5} = 0.5$$
$$\hat{\phi}_{12}^2 = \Phi_1^2(\boldsymbol{x}_2) = \frac{h_1(\boldsymbol{x}_2)}{h_1(\boldsymbol{x}_2) + \gamma h_2(\boldsymbol{x}_2)^2 + h_3(\boldsymbol{x}_2)} = \frac{0}{0+\gamma+0} = 0$$

where we notice that $\frac{2-\gamma}{2(2+\gamma)}$ is equivalent to β in the formulation.

As mentioned, we can derive the nodal values using various functions. Another example is

$$\Phi_K^I = \frac{W_K^I}{\sum_{J\in\mathcal{N}} W_J^I}$$
$$W_J^I = \begin{cases} \gamma\, h_J(x) & \text{for} \quad I = J \\ h_J(x) & \text{for} \quad I \neq J \end{cases} \tag{B.3}$$

in which $\frac{1-\gamma}{2(1+\gamma)}$ is equivalent to β of the formulation.

Next we show how Eq. (6) is reached for the triangular overlapping element. By definition, the ρ_K are

$$\begin{aligned} \rho_1 &= h_1\phi_1^1 + h_2\phi_1^2 + h_3\phi_1^3 \\ \rho_2 &= h_1\phi_2^1 + h_2\phi_2^2 + h_3\phi_2^3 \\ \rho_3 &= h_1\phi_3^1 + h_2\phi_3^2 + h_3\phi_3^3 \end{aligned} \tag{B.4}$$

Using the nodal values given in Appendix A, we obtain

$$\begin{aligned} \rho_1 &= h_1\left(\hat{h}_1 + A\hat{h}_4 + A\hat{h}_6\right) + h_2\left(\hat{h}_1 + B\hat{h}_4 + 0.5\hat{h}_6\right) + h_3\left(\hat{h}_1 + 0.5\hat{h}_4 + B\hat{h}_6\right) \\ \rho_2 &= h_1\left(\hat{h}_2 + B\hat{h}_4 + 0.5\hat{h}_5\right) + h_2\left(\hat{h}_2 + A\hat{h}_4 + A\hat{h}_5\right) + h_3\left(\hat{h}_2 + 0.5\hat{h}_4 + B\hat{h}_5\right) \\ \rho_3 &= h_1\left(\hat{h}_3 + 0.5\hat{h}_5 + B\hat{h}_6\right) + h_2\left(\hat{h}_3 + B\hat{h}_5 + 0.5\hat{h}_6\right) + h_3\left(\hat{h}_3 + A\hat{h}_5 + A\hat{h}_6\right) \end{aligned} \tag{B.5}$$

But the $\hat{h}_1$, $\hat{h}_2$, and $\hat{h}_3$ can be expressed as [12]

$$\begin{aligned} \hat{h}_1 &= h_1 - 0.5(\hat{h}_4 + \hat{h}_6) \\ \hat{h}_2 &= h_2 - 0.5(\hat{h}_4 + \hat{h}_5) \\ \hat{h}_3 &= h_3 - 0.5(\hat{h}_5 + \hat{h}_6) \end{aligned} \tag{B.6}$$

where $\hat{h}_4 = 4h_1h_2$, $\hat{h}_5 = 4h_2h_3$, and $\hat{h}_6 = 4h_3h_1$.

Substituting Eq. (B.6) into Eq. (B.5), we obtain

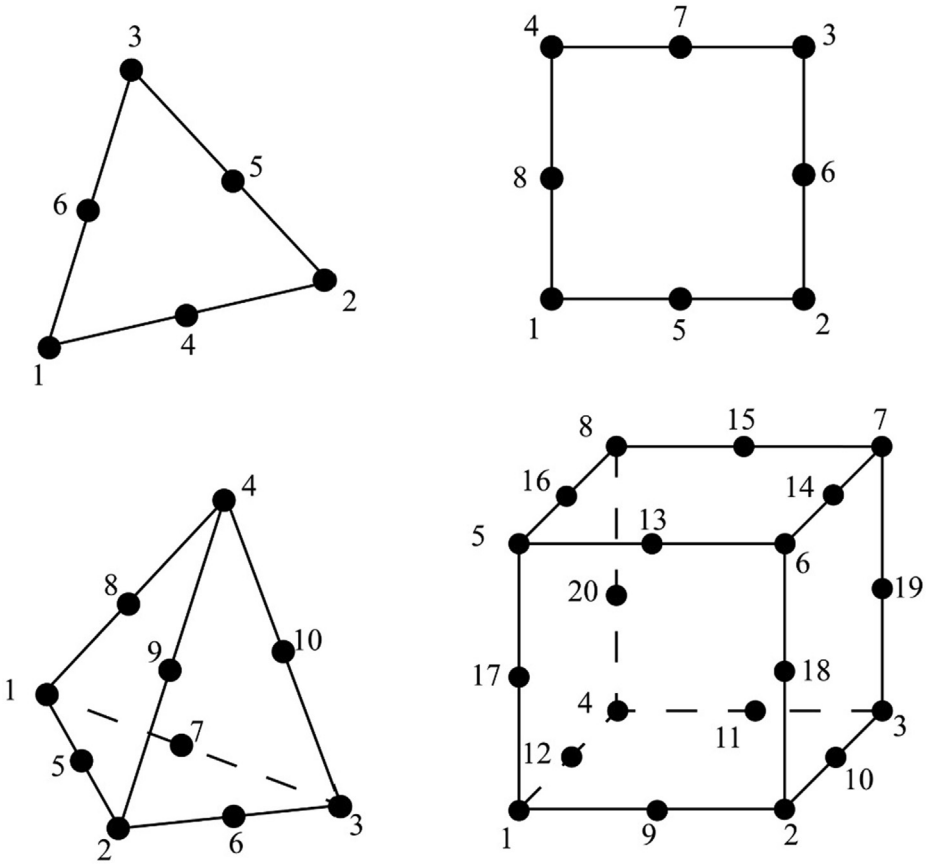

Fig. A1. Node numbering for the new overlapping finite elements.

$$\begin{aligned}
\rho_1 &= h_1\left(h_1 + (A-0.5)\hat{h}_4 + (A-0.5)\hat{h}_6\right) + h_2\left(h_1 + (B-0.5)\hat{h}_4\right) \\
&\quad + h_3\left(h_1 + (B-0.5)\hat{h}_6\right) \\
\rho_2 &= h_1\left(h_2 + (B-0.5)\hat{h}_4\right) + h_2\left(h_2 + (A-0.5)\hat{h}_4 + (A-0.5)\hat{h}_5\right) \\
&\quad + h_3\left(h_2 + (B-0.5)\hat{h}_5\right) \\
\rho_3 &= h_1\left(h_3 + (B-0.5)\hat{h}_6\right) + h_2\left(h_3 + (B-0.5)\hat{h}_5\right) \\
&\quad + h_3\left(h_3 + (A-0.5)\hat{h}_5 + (A-0.5)\hat{h}_6\right)
\end{aligned} \tag{B.7}$$

Then substituting $A = 0.5 - \beta$ and $B = 0.5 + \beta$

$$\begin{aligned}
\rho_1 &= (h_1 + h_2 + h_3)h_1 + \beta(h_2 - h_1)\hat{h}_4 + \beta(h_3 - h_1)\hat{h}_6 \\
\rho_2 &= (h_1 + h_2 + h_3)h_2 + \beta(h_1 - h_2)\hat{h}_4 + \beta(h_3 - h_2)\hat{h}_5 \\
\rho_3 &= (h_1 + h_2 + h_3)h_3 + \beta(h_2 - h_3)\hat{h}_5 + \beta(h_1 - h_3)\hat{h}_6
\end{aligned} \tag{B.8}$$

Since $h_1 + h_2 + h_3 = 1$ we have Eq. (6)

$$\begin{aligned}
\rho_1 &= h_1 + \beta(h_2 - h_1)\hat{h}_4 + \beta(h_3 - h_1)\hat{h}_6 \\
\rho_2 &= h_2 + \beta(h_1 - h_2)\hat{h}_4 + \beta(h_3 - h_2)\hat{h}_5 \\
\rho_3 &= h_3 + \beta(h_2 - h_3)\hat{h}_5 + \beta(h_1 - h_3)\hat{h}_6
\end{aligned} \tag{B.9}$$

Eq. (6) is obtained similarly for the other elements.

References

[1] Bathe KJ. The AMORE paradigm for finite element analysis. Adv Eng Softw 2019;130:1–13.
[2] De S, Bathe KJ. The method of finite spheres. Comput Mech 2000;25:329–45.
[3] Chen JS, Hillman M, Chi SW. Meshfree methods: progress made after 20 years. J Eng Mech 2017;143(4):04017001.
[4] De S, Bathe KJ. Towards an efficient meshless computational technique: the method of finite spheres. Eng Comput 2001;18:170–92.
[5] Nguyen VP, Rabczuk T, Bordas S, Duflot M. Meshless methods: a review and computer implementation aspects. Math Comput Simul 2008;79:763–813.
[6] Babuška I, Banerjee U, Osborn JE, Zhang Q. Effect of numerical integration on meshless methods. Comput Methods Appl Mech Eng 2009;198:2886–97.
[7] Bathe KJ. The finite element method with "overlapping finite elements". In: Zingoni A, editor. Proceedings sixth international conference on structural engineering, mechanics and computation – SEMC 2016, Cape Town, South Africa.
[8] Bathe KJ, Zhang L. The finite element method with overlapping elements – a new paradigm for CAD driven simulations. Comput Struct 2017;182:526–39.
[9] Zhang L, Bathe KJ. Overlapping finite elements for a new paradigm of solution. Comput Struct 2017;187:64–76.
[10] Zhang L, Kim KT, Bathe KJ. The new paradigm of finite element solutions with overlapping elements in CAD – computational efficiency of the procedure. Comput Struct 2018;199:1–17.
[11] Huang J, Bathe KJ. Quadrilateral overlapping elements and their use in the AMORE paradigm. Comput Struct 2019;222:25–35.
[12] Bathe KJ. Finite element procedures. Prentice Hall; 1996. 2nd ed. KJ Bathe, Watertown, MA; 2014, and Higher Education Press, Beijing; 2016.
[13] Strouboulis T, Babuška I, Copps K. The design and analysis of the generalized finite element method. Comput Methods Appl Mech Eng 2000;181:43–69.
[14] Tian R, Yagawa G, Terasaka H. Linear dependence problems of partition of unity-based generalized FEMs. Comput Methods Appl Mech Eng 2006;195:4768–82.
[15] Kim S, Lee PS. A new enriched 4-node 2D solid finite element free from the linear dependence problem. Comput Struct 2018;202:25–43.
[16] Kim S, Lee PS. New enriched 3D solid finite elements: 8-node hexahedral, 6-node prismatic, and 5-node pyramidal elements. Comput Struct 2019;216:40–63.
[17] Hong WT, Lee PS. Mesh based construction of flat-top partition of unity functions. Appl Math Comput 2013;219:8687–704.
[18] Zhang Q, Banerjee U, Babuška I. Higher order stable generalized finite element method. Numer Math 2014;128:1–29.
[19] Kim J, Bathe KJ. The finite element method enriched by interpolation covers. Comput Struct 2013;116:35–49.
[20] Kim J, Bathe KJ. Towards a procedure to automatically improve finite element solutions by interpolation covers. Comput Struct 2014;131:81–97.
[21] Jeon HM, Lee PS, Bathe KJ. The MITC3 shell finite element enriched by interpolation covers. Comput Struct 2014;134:128–42.

[22] Cowper GR. Gaussian quadrature formulas for triangles. Int J Numer Methods Eng 1973;7:405–8.
[23] Keast P. Moderate-degree tetrahedral quadrature formulas. Comput Methods Appl Mech Eng 1986;55:339–48.
[24] Yu J. Symmetric Gaussian quadrature formulae for tetrahedronal regions. Comput Methods Appl Mech Eng 1984;43:349–53.
[25] Lee NS, Bathe KJ. Effects of element distortions on the performance of isoparametric elements. Int J Numer Methods Eng 1993;36:3553–76.
[26] Huang J, Bathe KJ. On the convergence of overlapping elements and overlapping meshes. Comput Struct 2021;244:106429.
[27] MacNeal RH. A theorem regarding the locking of tapered four-noded membrane elements. Int J Numer Methods Eng 1987;24:1793–9.
[28] Bucalem ML, Bathe KJ. The mechanics of solids and structures – hierarchical modeling and the finite element solution. Springer; 2011.